Chapter 8
Molecular Dynamics Simulations

8.1 Molecular Dynamics Simulations in Ionic Systems

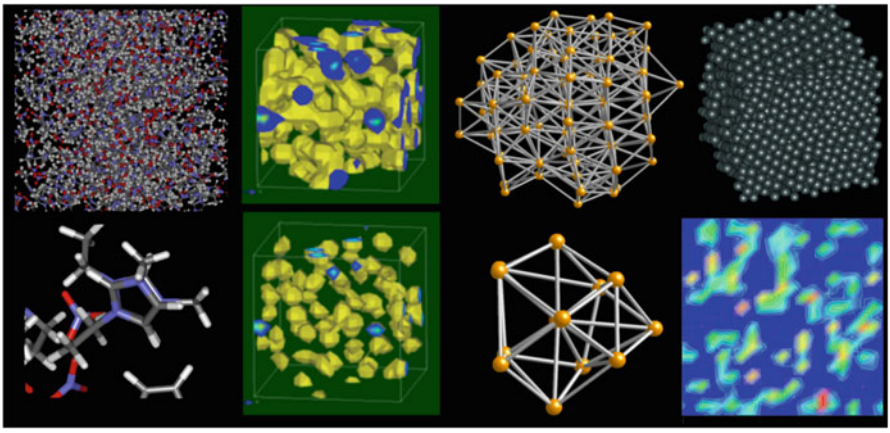

8.1.1 Purpose and Goals of the Molecular Dynamics Simulations

Molecular dynamics (MD) simulations are one of the methods of the computational science. One can study the structure and dynamics of the system in the computer by solving the equation of motion. Utilization of MD simulations has spread over many fields, such as biophysics, drug designs, as well as fundamental research areas in chemistry and physics. Systems and materials covered include proteins, liquid crystals, colloidal systems, polymers, glass-forming liquids.

The purpose of the simulation is not necessarily the faithful reproduction of the real system. Simulation is also used to examine the essential part of the dynamics

J. Habasaki et al., *Dynamics of Glassy, Crystalline and Liquid Ionic Conductors*,
Topics in Applied Physics 132, DOI 10.1007/978-3-319-42391-3_8

and/or structures of the model, and such a simulation is not required to be fully realistic. Therefore, it is necessary to understand the possible limitations of the methods and judging them according to the purpose. As already mentioned, MD simulations can treat the dynamics, because the equation of motion is numerically solved. For other properties such as equilibrated structures, the results of MD simulations are compatible with those by the Monte Carlo (MC) method.

Some of possible purposes, for which MD simulations are favorable or useful, are given as follows.

1. Simulation can be used to examine some commonly recognized as the essential parts of the dynamics and/or structures, such as the mechanism of ion diffusion and conductivity, the glass transition, the mixed alkali effects, the non-exponentiality and dynamical heterogeneity of the ion dynamics.
2. Simulations can be used for the prediction of the properties of systems not previously known by experiments. Simulations can provide properties not easily accessible by experiments such as the spatial information from wave number (q)-dependence of the intermediate scattering function.
3. Simulations can be used to examine systems under more extreme conditions including high pressures and high temperatures, which might be difficult to reach by experiments.
4. Sometimes, real experiments bring environmental pollution by the emission of heat, effusion of materials, and they might be hazardous. Simulations can examine the systems without environmental pollution or such danger.
5. Simulations can be used for screening various systems in the search for desired properties. In such cases, crude levels of the simulations are not necessarily a drawback, particularly if the time required is short.
6. Simulations can be used to treat changes of properties of systems when the structure, composition, mass, size, and/or other parameters, is modified.
7. Simulations can be used systematically to design new materials with improved performance in applications.
8. Of course, simulations can be used for comparison with the results obtained from experiments, and for validation of predictions from theory. Recently, they are also used to be a basis of construction and/or refinement of theories and models.

In the field of ionics, they are also applied for understanding dynamics and structures of new materials as well as composites or functional materials such as solid state batteries, actuators, and nano-machines in recent works and will be more applied in future works. It is expected that applicability of MD simulations will spread over wider fields of both fundamentals and applications.

8.1.2 History of MD Simulations in Ionics

Applications of MD simulations to ionics have a long history, and some early developments are introduced here. As far as we know, the first MD work for ionic

system seems to be that by Woodcock in 1971 [1], in which alkali chlorides in the liquid state are treated by using the empirical potentials by Tosi and Fumi [2, 3]. Soon after, Rahman et al. [4] examined the structure and motion in liquid BeF_2, $LiBeF_3$ and LiF, assuming purely ionic interactions. It is worth to mention that the former two systems can be regarded a model of silica and silicate, because of comparable size ratio of constituent atoms. After these works, vitreous state for silica was examined by Woodcock et al. [5], where even individual motions of Si and O atoms were examined. Soules also examined the structure and dynamics of glasses including silicate [6]. These pioneer works of MD and/or Monte Carlo Simulation (for example see Ref. [7]) take important roles to understand the structure and dynamics of ionic systems including those in the glassy states.

Although the formal charge models used in almost of early works can pick up some essential character of the ionic motion or structures, still they were not good enough for comparison with experimental ones. A large discrepancy can be found in formal charge model. For example, the glass transition temperature, T_g, tends to be extremely different, and/or pressure becomes several orders larger or smaller than the ambient pressure. Therefore, the history of classical MD simulations is also a history of developments of reliable potential parameters, when used for comparison with experiments. The system size and time scale covered were limited in early works due to the limited power of computers. Furthermore, treatment of Coulombic force needs larger cost of calculation than with repulsive force of short length scale. As a result, the simulation times of early works on ionic systems were of the order of several pico seconds and the system size was also small (~several hundreds). This limitation of size and time scale caused several problems such as undesirable effect of periodic boundary conditions, insufficient equilibration time and insufficient sampling of rare events. In spite of such limitations, many new insights had been brought forth.

Empirical potential model for MD was usually derived from the information on crystal structures and related information such as compressibility, expansivity, structure of polymorphs. Although the models enable important tasks to be carried out by simulations, more realistic potential models have been sought after, since the quality of the available models was not necessarily good enough for some purposes. Many researchers have tried the determination of better potential parameters for different systems. Modeling by *ab-initio* quantum mechanical potential surfaces has been used for calculations in physics by several authors. In 1988, the simple pair additive potential derived from the quantum mechanical calculation was shown to be effective enough to reproduce polymorphs of silica by Tsuneyuki et al. [8, 9] (hereafter referred to as TTAM). Effective parameters used to reproduce the several Mg silicates were also derived by them using the potential energy surfaces of model clusters of both SiO_2 and MgO. Their method for the silicate is applicable only when the condition $q\mathrm{M} = -q\mathrm{O}$ is a good approximation, where q is the charge number. In 1990, the progress of the modeling methods in mineralogy has been reviewed by Catlow and Price [10]. Thus far, many MD works have been done for ionic systems for both molten [11] and glassy states using several kinds of potential parameters.

Although alkali silicates are typical glass-forming materials and a study of the structures and properties is important not only for industrial use but also for the fundamental understanding of minerals, ceramics and glasses, an adequate potential model for predicting the unknown properties had not yet been established for a long time. In 1992, Habasaki and Okada derived parameters for some alkali silicates [12], which have a different stoichiometry from Mg silicates, based on the ab initio MO calculation (see Sect. 9.1), by using the method similar to the approach in deriving TTAM. Because of the additivity of the different atomic species, the parameters are suitable for the study of the mixed alkali effect as well (see Chap. 10). The effect was reproduced by MD simulations successfully and jump paths (ion channels) for ionic motion were visualized for the first time as far as we know [12–14] and elaborated further in Refs. [15, 16]. Dynamic heterogeneity in the ionically conducting glass is observed in the motion of Li ions in lithium metasilicate [17, 18]. (See Sects. 9.5 and 11.5 for details.) This characteristic property is shared by structural relaxation of glass forming liquids, and the commonality has drawn attentions in the relation with the mechanism of the glass transition. Nowadays, the potential parameters are widely used by several other groups [19–22].

MD simulations have been used to examine a variety of nature of ionic systems. Using small angle X-ray diffraction and MD simulations, Greaves [23] has shown the clustering of alkalis in mixed alkali disilicate. By Jund et al. [24] and by Horbach and Kob [25], channel diffusion of sodium in silicate glass and melt was examined, and the relationship with the mode coupling theory also was discussed [26, 27]. Details of structures and dynamics are also examined in related systems. Recently, ionic liquids are actively examined by MD simulations and many common views with glass forming liquids are reported (see Chap. 11 for details).

With rapid developments of computer and technology for acceleration of calculations, the classical MD can now cover wider range of materials, compositions, temperatures, pressures and time scales. In recent years, ab initio molecular orbital (MO) calculation or calculation by density functional theory (DFT) can be done for the relatively larger systems [28, 29]. Furthermore, works using ab initio MD went the dawn, although some cautions might be necessary for the treatment of it, especially for the case of the slow dynamics as discussed in the next section.

Using ab initio MD methods, Tilocca [29] has examined the phosphosilicate glass, which is bioactive material. Recently, Payal and Balasubramanian [30] have performed the ab initio MD of dissolution of cellulose in ionic liquids. Such works will increase the importance and reliability with further development of computer technology in enabling the larger size and longer time scale calculations.

8.2 Methods in Molecular Dynamics Simulations

Nowadays, many MD programs are available and researchers are not necessarily to be programmers themselves. However, the contents of programs aimed for general purposes tend to be too complicated and often they seem to be a black box. In this

section, the essence of methods used in the molecular dynamics simulation is explained, enabling the reader to understand the outline of it, and what is done in the programs. Our attention is mainly focused on the treatment of ionic systems by classical MD. In Chap. 12, practical introduction for MD simulations is given with some examples of the treatments of MD data.

For planning research using MD, the researcher is recommended to consider the characteristics of the problem to be examined as well as requirements of system size and time scale carefully. Then one can choose the most suitable method within the available resources, because classical and *ab-initio* methods as well as other methods all have their own advantage and limitation. Although needless to say, for a meaningful comparison of methods, reasonable choices of initial configurations, equilibration, suitable choice of conditions such as cooling schedules as well as good statistics are required. Therefore careful judgment for the usefulness and limitations of them is required. Even in the classical method, the covered space and time region might not be large enough, and consequently the results are problematic in such cases. This problem appears remarkably in ab initio MD, which requires larger calculation cost and also the "real time" required for the calculations. The problem will be discussed in the following section.

8.2.1 Classical and Ab Initio Methods

Here we compare classical and ab initio methods in the study of ionics briefly, although mainly the former method is treated in the present book. In classical MD simulations, equations of motion are solved numerically, based on a given potential model. When large scale simulations of long time are necessary, classical MD using empirical force field or effective force field derived from the ab initio molecular orbital calculation or density functional calculations are the practice because of lower calculation costs and time. For realistic simulations comparable to experiment, potential parameters with good quality are required; however, researchers of classical MD often encounter a problem of "missing parameters". Situation becomes worse in the complex systems with many interactions. In such works, it is difficult to find out suitable parameters and their combinations for the system to be examined. Although there are several approaches to treat general parameters and/or combination rules, careful judgement for the quality of the potential model is necessary. In such cases, derivation of suitable parameters for each problem is expected. Thus, in the classical MD simulations or hybrids of quantum and classical methods, one needs to critically examine the quality of the potential parameters, and the functions used, as well other conditions. Of course, more realistic simulations are better for some purposes. Ab initio MD methods such as the Car-Parrinello (C-P) methods [2] are contributing to recent developments of the computational science. In C-P, electrostatic states of the system are calculated using the density functional theory (DFT) with solving the equation of motions, at the same time. The method is particularly applicable if there are the time dependent changes

of electronic states during the simulation as in the case of occurring chemical reaction. It is useful to examine the structures and dynamics in details, provided suitable conditions are fulfilled. Considering above situation, one may consider that the ab initio method is always the best choice. However, tractable ab initio methods have serious limitation in the following situations. In the case of ion dynamics in ionically conducting in molten and glassy states or in ionic liquids, dynamics observed are slow, similar to the super cooled liquids near the glass transition temperature [31], and therefore long time simulations as well as large size are required. Unfortunately, it is not easy to perform ab initio MD in suitable conditions, because of huge calculation resources and time required. For example, activation energy obtained from the short time ab initio MD seems to be used as a guide of material designs such as lithium batteries [32]. Although such approaches are useful, one should note that the obtained short time activation energy is for each jump motion and is not the same as that for diffusion (and/or conduction) of long time scale (see Sect. 9.4.2), in the case of densely packed materials such as supercooled liquids, crystals and glasses. That is, long time scale is required to examine transport properties in low temperature regions or in high pressure regions. In recent works in ab initio MD, typically system containing tens to hundreds particles during several ps ~ several tens of ps are examined. In contrast, in classical MD simulations of ionic systems, typically several thousand ~ several tens of thousands particles during ns ~ several tens of ns are examined. This situation of ab initio MD is similar to that in the beginning of the classical MD, where many problems were found due to the limited system sizes and the limited simulation time. Because of such limitations of *ab-initio* MD, the result obtained for slow dynamics in some systems may not be reliable, although challenges to larger system and longer time scale are continuing. The difference of several orders of magnitude in time scales and system size of the two methods are non-negligible and it will not be removed easily even by the further development of the computational technology. Nowadays, such limitation of ab initio MD seems to begin to be recognized well and many kinds of hybrid methods or combinations of methods tend to be used for each targeted problem. For the treatment of slow dynamics, classical MD simulation using the potential (force field) based on the ab initio MO calculation or DFT is a one of the suitable approaches for covering longer time region and larger system size with a relatively low cost. Our and related works using the approach will be explained in the Chaps. 9–11. When the potential curves or surfaces are not time dependent, classical MD simulations using reliable potential are good enough to examine the structure and dynamics of systems. Thus when applied to model systems, this method is capable of generating a "computational experiment" to uncover the principles of structure formation and/or the mechanism of the dynamics under well controlled conditions. In the studies of ionics in glasses [33–35] and ionic liquids [36], comparisons of ab initio and classical methods are reported. Pópolo et al. have argued that the local structure around the cation obtained from ab initio MD in dimethyl imidazolium chloride [DMIM][Cl] shows significant differences compared to both the classical calculations and the neutron results [36]. The author suggests ways in which the classical potentials may be

improved. Recently, Carré et al. [37] derived the effective potential for silica based on the C-P MD [38] amenable for the larger and longer scale simulations. On the other hand, classical MD can also provide initial configurations for ab initio MD simulations, MO and DFT calculations, after long time equilibration. In this sense, both methods are complementally each other. Other approaches to cover the long time and large system size are also in progress. In the case of ionic liquids which have inner structures, coarse-grained models [39, 40] are the possible choices to extract the essential part of the structure or dynamics besides the fully atomistic simulations.

8.2.2 Models Used in MD Simulations

Potential functions and their parameters are the main "input" of the MD simulation, which determine the characteristics of the system. Here typical models used in the classical MD are summarized. Several functional forms of potential (force field) are used for MD simulation. Soft-sphere and Lennard-Jones are frequently used as model systems for examining liquids, crystals and glasses including the problem of the glass transition. They are also used as a part of ionic models having more complicated form. For the simulation of realistic systems, unknown parameters can be determined from the experimental data such as expansibility, compressibility, structures and/or from quantum mechanical methods.

8.2.2.1 Soft-Sphere Model

The model consists of the repulsive term in the following form [41–47] is traditionally called as soft-core (SC) model.

$$\varphi_{ij} = \varepsilon\left(\frac{\sigma}{r_{ij}}\right)^{n}, \tag{8.1}$$

where the r_{ij} is the distance between particle i and j. The parameter ε, and σ determine the depth and the size of the potential well, respectively. The reduced units are often used for describing general properties and for comparison with results. For example, the reduced unit of length, l $(= (V/N)^{1/3})$, and time τ $(=l(m/\varepsilon)^{1/2}(l/\sigma)^{n/2})$ are used, so that the equation of the motion becomes simple. Here V, N and m stand for system volume, total number and mass of particle, respectively.

Recently, this functional (inverse power law) form is considered as a basis for understanding the thermodynamic scaling (TV^{γ} scaling) of dynamical properties known for many systems including ionic liquids [48] and ionically conducting systems and importance of the model seems to be increasing (see Chap. 7). In the

scaling law for the inverse power law (SC) potential, exponent n in Eq. (8.1) is connected to γ value of the system.

The SC system satisfies "dynamical scaling law" [44, 45], which is an extension of the scaling law of the hard sphere (HS) system. For the HS system, one considers N hard spheres of radius σ in the box of volume V ($=L^3$) and starts to move with given initial coordinates and velocities. If the initial coordinates, velocities, L, and σ are multiplied by a constant C (>0), the trajectory in the configuration space of $3N$ dimension is similar to that of the original one. If only the initial velocities are multiplied by C, the trajectory is unchanged through time intervals between collisions and is reduced by the factor of $1/C$. This is the dynamical scaling law of the HS system. In a similar manner, in the SC model, dynamic scaling law holds exactly and even a non-equilibrium relaxation can be represented by analytical expression.

In experiments, going back to the early days, several one component systems such as glycerol and/or ethanol are known to be excellent glass formers [49–51] and the simplicity of the one component system was recognized in the study of the glass transition problem. However, in early MD works around 1970, one-component SC system was found to crystallize within a short run, and hence binary system tends to be used for the study of glass transition [52–54]. In spite of this historical situation, one-component SC system can be a good model to study glass transition due to its simple theoretical treatment, if the crystallization is suppressed. Fortunately, when the system size is large enough (>500), the crystallization seem to be suppressed at long time and almost systems become metastable ones after non-equilibrium relaxation [45]. Actually, in many runs in the system larger than 2000 particles, one-component SC model with $n = 12$ shows non-equilibrium relaxation towards metastable states (called as a glass branch), which can be regarded as the (stabilized) glassy states, from both structural [45] and thermodynamical [46] properties. In the metastable glassy state, different local structures (face-centered cubic (fcc) like and body-centered cubic (bcc) like) are found to be mixing. Because of the mixing of different local structures, disordered structures can be formed without introducing different kinds of particles to form binary systems. Thus the glass transition can be mapped on a phase-diagram using the compressibility factor plotted against reduced density. When the system is rapidly quenched along the liquid branch of the phase-diagram, the system tends to be trapped on the midway towards the glass branch.

Recently, several one component systems including the ones with special types of potential functions are examined to understand the glass transition [55, 56].

8.2.2.2 The Lennard-Jones Model

The Lennard-Jones (LJ) model [57] has the following form.

$$\phi(r_{ij}) = 4\varepsilon\left[\left(\frac{\sigma_{ij}}{r_{ij}}\right)^{12} - \left(\frac{\sigma_{ij}}{r_{ij}}\right)^{6}\right], \tag{8.2}$$

The function becomes 0 at $r_{ij} = \sigma$ and the minimum is observed at $r_{\mathrm{ij}} = \sqrt[6]{2}\sigma$, where the function becomes $-\varepsilon$. The former is regarded as the size of the particle, and therefore, σ is used as a unit of length r.

The parameters for argon, $\sigma = 3.405$ Å and $\varepsilon/k_{\mathrm{B}} = 119.8$ K, where k_{B} is the Boltzmann constant, have been used in many theoretical works [58]. Several new parameters are proposed for argon (or other materials). The values $\sigma = 3.345$ Å and $\varepsilon/k_{\mathrm{B}} = 125.7$ K bring a better agreement between theory and experiment for thermodynamic behaviors of the system [59]

Generalized forms of LJ model [60, 61] consists of repulsive and attractive terms,

$$\phi(r_{ij}) = 4\varepsilon\left[\left(\frac{\sigma_{ij}}{r_{ij}}\right)^{n} - \left(\frac{\sigma_{ij}}{r_{ij}}\right)^{m}\right] \tag{8.3}$$

with powers n and m replacing the 12 and 6 respectively are also used in recent studies of the dynamics of glass-formers.

Binary LJ System

In recent years, starting from the study by Kob and Andersen, binary systems of LJ systems have been used as a model system exhibiting the glass transition and there are accumulated numbers of MD works based on these systems [62–65]. Bordat et al. have compared three different interaction models [63, 64], where the structures and dynamics of the system composed of 1500 particles (1200 for species A and 300 for species B) are discussed related to the glass transition problem. General forms of the binary LJ used in their work are represented by

$$V(r) = \frac{E_0}{(q-p)}\left[p\left(\frac{r_0}{r}\right)^{q} - q\left(\frac{r_0}{r}\right)^{p}\right], \tag{8.4}$$

where E_0 and r_0 are respectively a parameter for energy depth and position of the minimum of the potential well. In the model I, $q = 12$ and $p = 11$. In the model III, $q = 8$ and $p = 5$. The parameters for $q = 12$ and $p = 6$ for model II corresponds to the Kob-Anderson model [62], which has been extensively examined as a model of glass transition (see Table 8.1).

The anharmonicity of the potential for A-A interaction is increasing in the order of I (12-11), II (12-6) and III (8-5). The 'fragility' obtained from several methods is increasing in order of I, II and III. It parallels to the change of stretching exponent β of I, II and III, which are 0.69, 0.65 and 0.60, respectively. That is, the capacity of

Table 8.1 Parameters of the Lennard-Jones potentials in the Kob-Andersen model, where ($\sigma = \frac{r_0}{2^{1/6}}$) in Eq. (8.4)

Interaction	A-A	B-B	A-B
E_0	1.0	0.5	1.5
σ	1.0	0.88	0.8

intermolecular coupling and anharmonicity of the potential has the effect in increasing fragility and the non-exponentially parameter $(1-\beta)$, which is the same as the coupling parameter, n, in the coupling model.

Even for the binary LJ systems, one may expect the existence of some mixing effect for the dynamics and structures. This is because the glassy system like silicates shows a large non-linear change of the dynamics by mixing of different kind of alkali ions, known to be "mixed alkali effect" (see Sect. 4.8 and Chap. 10). In this case, it was well established that the mixing of different sizes of alkali metal ions causes the mutual interception of jump paths in a certain time scale and suppression of the cooperative motion which enhances the effect [65]. For example, in the case of lithium potassium silicates, mutual interception means that the Li ion cannot enter the site previously occupied by K ion, while K ion cannot enter the site previously occupied by Li ion. Similar situations are found in the generalized LJ mixtures [66, 67]. The ionic liquids also can be regarded as the binary system of cation and anion. Comparison of generalized binary Lennard-Jones (LJ) systems with different potential parameters is helpful to understand the dynamics of ionic liquids, especially for the physical meaning of the coupling of the anion and cation or the role of charges [31].

Other functional forms used in inorganic materials especially for Ionics will be introduced hereafter.

8.2.2.3 Huggins-Mayer Potential

Fumi and Tosi [3, 68] developed potential parameters for alkali halide such as NaCl, by fitting the Huggins-Mayer dispersive energy to crystallographic data. The function form is as follows.

$$\varphi(r_{ij}) = A_{ij}e^{-\frac{r_{ij}}{\sigma_{ij}}} - \frac{C_{ij}}{r_{ij}^6} - \frac{D_{ij}}{r_{ij}^8} + \frac{q_i q_j}{4\pi\varepsilon_0\, r_{ij}}, \tag{8.5}$$

where the exponential term is for repulsive interaction, while inverse power-law terms represent the attractive interaction. A_{ij} is called the Pauling factor, defined by $1 + Z_i/n_i + Z_j/n_j$, where n_i is number of electron of the most outer shell of the ion i and Z_i is for electric charge on species i. The second and third term is for dipole-dipole and dipole-quadrupole interactions, respectively. The fourth term for the right hand side is for Coulombic interaction term with charges q.

Several functional forms for ionic systems are suggested so far, and both empirical and ab initio based potential parameters are developed.

8.2.2.4 Born-Mayer-Huggins Potential

The following similar in form to the previous one is called as Born-Myer-Huggins model.

$$\varphi(r_{ij}) = A_{ij}e^{\frac{\sigma_i+\sigma_j-r_{ij}}{\rho}} - \frac{C_{ij}}{r_{ij}^6} - \frac{D_{ij}}{r_{ij}^8} + \frac{q_i q_j}{4\pi\varepsilon_0 r_{ij}} \tag{8.6}$$

The first term on the right-hand side represents the Born-Myer repulsive term. The value of r represents the distance between atoms, and σ_i is a size of i ion. Here, ρ is the softness parameter.

8.2.2.5 Gilbert-Ida Type Potential

Gilbert-Ida type [69, 70] repulsive potential combined with Coulombic force has been successfully used for silica [8] and lithium, sodium and potassium silicates [12]. It is given by

$$\phi(r_{ij}) = \frac{q_i q_j}{r_{ij}} + f_0(b_i + b_j)\exp\left(\frac{a_i + a_j - r_{ij}}{b_i + b_j}\right) - c_i c_j r_{ij}^{-6} \tag{8.7}$$

The first term on the right-hand side represents the Coulombic interaction. The value of r_{ij} (Å) represents the distance between atoms, and a_i (Å) and b_i (Å) are the effective radius and the softness parameter, respectively, of atom i. the value f_0 is a constant (=1 kcal mol^{-1} Å^{-1}). The parameters $c_i c_j$ (kcal Å^6 mol^{-1}) are for the correction of the curvature for the interaction of pairs including oxygen atom, and therefore may be treated as a part of repulsive potential term. Units in the function are as in original papers [8, 12], to avoid the loss of numerical accuracy by changing units. This potential form is additive for pair as well as atomic species. The latter property enables us to treat the mixed alkali system while keeping consistency with the single alkali systems. Therefore it is useful to study the "mixed alkali effect" (see Chap. 10). Examples of MD simulations of silicate crystals and glasses using this kind of potential will be shown in Chap. 9.

8.2.2.6 Potential Including Inner Structures

The following potential forms for representing both intermolecular and intramolecular interactions are frequently used for organic systems as well as ionic liquids [31, 71–73].

$$U(R) = \sum_{\text{bonds}} K_{\text{r}}\left(r - r_{\text{eq}}\right)^2 + \sum_{\text{angles}} K_{\theta}\left(\theta - \theta_{\text{eq}}\right)^2 + \sum_{\text{dihedrals}} \frac{V_{\text{n}}}{2}\left(1 + \cos\left[n\phi - \gamma\right]\right) + \sum_{\text{i<j}}^{\text{atoms}} \left(\frac{A_{\text{ij}}}{R_{\text{ij}}^{12}} - \frac{B_{\text{ij}}}{R_{\text{ij}}^{6}}\right) + \sum_{\text{i<j}}^{\text{atoms}} \frac{q_{\text{i}} q_{\text{j}}}{\varepsilon R_{\text{ij}}} \tag{8.8}$$

The model uses a sum of bond, angle, and dihedral deformation energies, a pairwise standard (6,12) Lennard-Jones potential, and Coulombic interactions between atoms with charges q_{i} and q_j.

Our and related works for ionic liquids using MD simulations are shown in Chap. 11.

8.2.2.7 Reactive Force Field

Reactive force fields, such as ReaxFF, have been used in several related works [74, 75], where the charge on the atom changes with the position. Such approaches will be useful in the investigation of the details of reactions on the surfaces of colloids, gels or related systems.

Other MO or DFT based potential model may be applicable for representing bond breaking of reconnection even if the charge seems to be fixed in the simulation. Actually, Habasaki and Ishikawa have observed that the clusters or gels can be formed in silica colloid-water-salt system [76] using the silica model by Tsuneyuki et al. [8] with a fixed charge. This is because the charge is fixed in the fitted parameters but not in the quantum mechanical calculations used for derivation of it. Therefore the model allows reconstruction of bonds.

8.2.2.8 Other Models

Models for Water

Many kinds of water model such as SPC, SPC/E [77, 78], TIPS3P, TIPS4P, TIPS5P [79, 80] are proposed so far. Comparison of some properties among different water models was reported in Refs. [81, 82]. Each model has both drawback and advantage and therefore researcher should select suitable one by any particular purpose. It may be useful for the researchers of glasses to mention that the structure and phase diagram of water is analogous to the silica due to network formation by hydrogen bonds in many points. Therefore, comparison of related systems will be useful for studies in both research fields.

8.2.3 Units Used in MD and Combination of Potential Models

It is recommended to use International System of Units (SI) in many fields; however, potential parameters or functions for MD simulations found in literatures are not necessarily given in SI. This is probably because values used in SI are not always appropriate for numerical treatments in order of magnitude. Many different units appear in MD programs and papers. Furthermore, reduced units are also used by physical reasons. Therefore, careful treatment of units is necessary. Because simulated systems are sensitive for the given potential parameters, it is better to avoid repeating conversions of units to keep numerical accuracy.

Quality of the potential parameters (for example, the size of the basis set used for derivation if it were based on ab initio MO calculation) should be good enough and comparable when one uses the combination of parameters taken from different sources. Sometimes, one may encounter the difficulty to combine the parameters because of different potential forms. In some cases, it is possible to change from one to the other. Gilbert-Ida type parameters can be easily changed to the Born-Mayer-Huggins form, although the merit of the additivity of the parameters is lost. The parameters in LJ form can be changed into those for Gilbert-Ida type, by a requirement of having the same energy minimum separation, depth and the same behavior for the large r region [83].

In treatment of ionic system (similar situation may happen in other systems), careful treatment of the term "mole" is required. For example, the system "Li_2SiO_3" is the same composition as "$x$$Li_2O$-$(1-x)$$SiO_2$" with $x = 0.5$. The former expression may be used to compare the different phases such as glass and crystal. The latter expression is often used for glasses to include composition dependence of the system. However, the system energy "per mole" for these system becomes different due to the different definition of "mole", because it is defined by the weight (represented by grams) of the Avogadro numbers of "specified groups of particles". In an MD program, the former expression may be chosen for mole because the smallest number of species (Si in this case) being an integer is preferred. In a certain MD program, ions included in a basic MD cell seem to be used as a group to define "mole". In ionic liquids, ion pair seems to be used as the group by many researches at least for simple systems. For comparison of works, it may be necessary to mention what unit is chosen for the definition of "mole" or changing the units to adjust it to conventional ones.

8.2.4 Solving the Equation of Motion

In principle, MD simulations describe the motions of particles (ions or atoms) by solving the equation of the motion. That is, the position of the particle is predicted from the previous and present ones by adding the forces acting from other particles.

In the case of classical MD, it would not be an exaggeration to say that potential functions and its parameters (force fields) determine the fate of the particles, if other conditions are reasonably selected.

The equation of the motion for i-th numbered particle can be written as,

$$\frac{d^2\mathbf{r}_i}{dt^2} = \frac{\mathbf{F}_i}{m}, i = 1, 2, \ldots N \tag{8.9}$$

8.2.4.1 Algorithm

In classical MD simulations, the equation of the motion is solved numerically. In other words, the next position of i-th particle is calculated based on the position at t and that of one or several steps before. Several algorithms to solve the equation of motions have so far been proposed. Here we explain the Verlet algorithm [84], which is simple and known to be symplectic [85, 86]. This method is suitable for calculation of motion including sudden changes of displacements (jumps or hops) found in melts and glasses, because it is not affected by the information of many steps before. The Gear's method, which is one of predictor-corrector methods with several steps, is also used for MD simulation [87]. In this case, slow dynamics by jump motions might be affected by the several steps before the motions. In other words, the method is not necessarily suitable when the sudden change occurs in the system. Although the method is known to be accurate in other cases and useful at least for a short time scale, drift of the motion might be non-negligible during long runs because of its non-symplectic nature.

In the Verlet method, the positions of i-th particle after Δt and that before Δt are

$$\mathbf{r}_i(t + \Delta t) = \mathbf{r}_i(t) + \Delta t\dot{\mathbf{r}}_i(t) + \frac{(\Delta t)^2}{2}\frac{\mathbf{F}_i(t)}{m} + O\left((\Delta t)^3\right) \tag{8.10}$$

$$\mathbf{r}_i(t - \Delta t) = \mathbf{r}_i(t) - \Delta t\dot{\mathbf{r}}_i(t) + \frac{(\Delta t)^2}{2}\frac{\mathbf{F}_i(t)}{m} + O\left((\Delta t)^3\right). \tag{8.11}$$

From the sum of Eqs. (8.10) and (8.11), one can obtain the following relation.

$$\mathbf{r}_i(t + \Delta t) + \mathbf{r}_i(t - \Delta t) = 2\mathbf{r}_i(t) + (\Delta t)^2\frac{\mathbf{F}_i(t)}{m} + O\left((\Delta t)^4\right), \tag{8.12}$$

On the other hand, from the difference of Eqs. (8.10) and (8.11), one can obtain the following equation,

$$\mathbf{r}_i(t + \Delta t) - \mathbf{r}_i(t - \Delta t) = 2\Delta t\dot{\mathbf{r}}_i(t) + O\left((\Delta t)^3\right), \tag{8.13}$$

That is, new position is,

$$\mathbf{r}_i(t+\Delta t) = 2\mathbf{r}_i(t) - \mathbf{r}_i(t-\Delta t) + (\Delta t)^2 \frac{\mathbf{F}_i(t)}{m} + O\Big((\Delta t)^4\Big), \tag{8.14}$$

and a new velocity is,

$$\dot{\mathbf{r}}_i(t) = \frac{1}{2\Delta t}\{\mathbf{r}_i(t+\Delta t) - \mathbf{r}_i(t-\Delta t)\} + O\Big((\Delta t)^2\Big), \tag{8.15}$$

A numerical error in solving equation of motion thus depends on the time of each step, Δt.

8.2.4.2 Periodic Boundary Conditions (PBC)

Periodic boundary condition (PBC) is frequently used in typical MD simulations of bulk systems. Schematic description of the periodic boundary conditions used in the simulations is shown in Fig. 8.1, where the basic cell containing particles is surrounded by the periodically repeating image cells infinitively.

The figure is for the two dimensional case; however, similar conditions are also used for three dimensional cases. (One should be careful to use 2D system for comparison with experiments except for a special purpose, because motions of atoms might be affected by the dimensionality of the space.) For a particle within

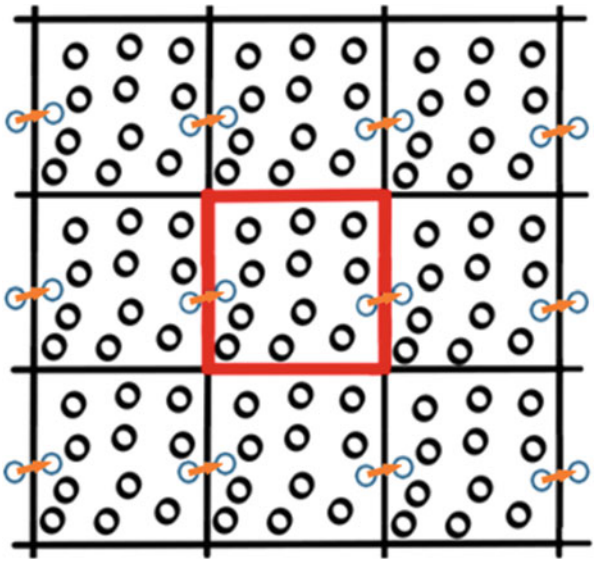

Fig. 8.1 Schematic description of the periodic boundary conditions used in the simulation. Image cells continue infinitively. When a particle moves out the basic cell of the MD simulation, another particle moves in from the image cell as shown by *orange arrows*

the basic cell, interactions from particles within the sphere with a certain cutoff length (typically chosen to be $L/2$, where L is a length of basic cell) are taken into account including ghost particles (images of the same particle found in the basic cell) in image cells.

By this treatment, we have the following benefit.

1. Properties of the bulk can be simulated by the limited number of particles. That is, effect of the surface can be removed.
2. If the particle moved beyond the boundary, the ghost particle comes into the basic cell. Therefore, in the case of constant number simulations such as NVE or NPT ensembles, the number of the particles is kept constant.
3. The periodicity like crystals makes it possible to calculate the long ranged Coulombic force using the Ewald method or related ones, even in the case of liquid or glasses. In many cases, minimum image (within $2/L$) is used for calculation of short range forces (and for real part of the Ewald summation explained later).

Following characteristics of the system should be kept in mind when one uses PBC. Even when we considered the infinitive system using PBC, the wave number accessible by the simulation is limited by the size of the simulation box. Furthermore, when one considered the motion of particle in the system with PBC, it is repeated as well and some artificial waves or vibrations in the particle motions will be formed. If the system size is too small, the particle might be affected by its own ghost in an image cell, which is moving in the same directions. Especially in the case of crystals, basic box of the MD is formed by several repeating basic lattices of the crystal and therefore the number of repetition of them in each axis direction will affect the periodicity of the motions. To reduce such effects, the system size used has to be large enough to the possible extent while ensuring the practical usability. It is useful to change the system size to check the effect.

For the study of glasses, further caution is required to avoid crystallization in the system. If only a small number of particles were contained in each basic box of the simulation, system may easily crystallize and/or behaves like crystals because of PBC. In the case of network glasses, long ranged oscillation tends to be formed and continued by PBC.

8.2.5 Treatment of Coulombic Force

Coulombic force is a long ranged force and has essential importance to consider in the ionic systems. The repulsive force is usually a short ranged force, and for it in MD simulations, using a certain cutoff length is a reasonable choice. Corrections by shifted force can also be used. The cutoff length should be chosen, so that the wave like structures of $g(r)$ for ion-ion converge (typically 8–15 Å). When the ion

(molecule or residue) has an inner structure, the distance among the center of unit structures can be considered as that for ionic structures.

As well known, the Madelung energy of simple crystal is represented as

$$E_{Madelung} = -N\alpha' Z^2 e^2 / r_0, \tag{8.16}$$

where α' is known to be Madelung constant [88]. The system energy is affected from the ions located at long distances. For isolated system such as small clusters or nano-crystals, one can use the direct sum or multipole expansion [89] of it.

If parameters and functions are given in SI, the Coulomb's constant is defined and given by $k = 1/(4\pi\varepsilon_0\varepsilon)$, where the constant ε_0 is the permittivity of free space and ε is a relative permittivity for the material concerned. The Coulombic potential formed by N ions around an ion is given by

$$\phi(r) = \frac{1}{4\pi\varepsilon_0} \sum_{n=1}^{N} \frac{q_n}{|r - r_n|}. \tag{8.17}$$

Convergence of the long range force for the Coulombic term needs a large cost in calculation. The calculation cost of direct sum of N particle is $N(N-1)$ when all combinations are counted, and is of the order of N^2 (i.e. $O(N^2)$). Order of N^2 means that, if the system size (particle number within the basic cell) is 100 times larger, the calculation cost is 10,000 times larger.

Coulombic force is treated by several methods in MD simulations as shown below.

8.2.5.1 The Ewald Method

The Ewald method [90–92] is a standard method for calculation of Coulombic term used in the MD simulations, which mimics the periodicity of the crystal structure by using a PBC of the MD cells. Many methods to reduce the cost have been developed and still are developing. Recently, particle-particle-particle-mesh (P^3M) Ewald [93, 94], particle mesh Ewald method (PME) [95], and multipole expansion method are also used. These methods will be explained in the following subsections.

In MD simulations of bulk system, all forces from the particles in the basic cell and those from image cells at infinitive distances are taken into account to eliminate surface effects. The Ewald method is applicable to both crystalline and non-crystalline materials such as liquids, super-cooled liquids and glasses. In non-crystalline systems, the method is used with the periodic boundary conditions (PBCs), where the system has a periodic charge distribution similar to crystals. With this condition, Coulombic potential of the system is represented by

$$\varphi_C = \frac{1}{2}\sum_{\mathbf{n}}\sum_{i}\sum_{j}{}' \frac{Q_i Q_j}{4\pi\varepsilon_0}\frac{1}{|\mathbf{r}_i - \mathbf{r}_j + \mathbf{Ln}|}, \tag{8.18}$$

where $\boldsymbol{L}$ is a vector to represent the size of basic cell of MD simulations and $\mathbf{n}$ is a vector consists of integers such as (1,1,1) to represent the image cells.

The summation for $\mathbf{n}$ is taken to consider the contribution of all image cells. The vector (0,0,0) mean a basic cell for the simulation and the term $(i = j)$ in the cell is excluded and this restriction is represented by Σ' in the summation.

The Ewald method takes into account infinitive numbers of ions using PBC without considering all image cells in the real space. In the method, Coulombic potential is separated into three parts, which is the real, the reciprocal and a constant (self) part as shown in the following equation.

$$\varphi_C = \varphi_{real} + \varphi_{recip} - \varphi_{self}. \tag{8.19}$$

The First Term of the Ewald Method, φ_{real}

Here we considered the j point charges around an ion "i". The first term φ_{real} is the sum of the real part for point charges around an "i" ion and the Gaussian distributions having the opposite sign for the system. The term for the real space is given by

$$\varphi_{real} = \frac{1}{2}\sum_i \sum_j{}' \frac{Q_i Q_j}{4\pi\varepsilon_0}\frac{erfc\left(\alpha\left|\boldsymbol{r}_i - \boldsymbol{r}_j\right|\right)}{\left|\boldsymbol{r}_i - \boldsymbol{r}_j\right|}. \tag{8.20}$$

Here the summation is taken for the sphere within a cut-off length, typically radius of $L/2$ from "i" particles, and not for all image cells. In the expression for φ_{real}, "erfc()" stands for the complementary error function defined by,

$$\mathrm{erfc}(\mathrm{x}) = 1 - \mathrm{erf}(\mathrm{x}) = \frac{2}{\sqrt{\pi}}\int_x^\infty e^{-t^2} dt \tag{8.21}$$

The term α in the expression is a setting parameter to determine the shape of the Gaussian distribution of the charge and also determines convergence of the term.

The Second Part of the Ewald Summation, φ_{recip}

A part not sufficiently taken into consideration in real space is compensated by the reciprocal lattice term φ_{recip}, which includes the Gaussian distributions having the same sign as the point charges considered, and is given by

$$\varphi_{recip} = \frac{2\pi}{V} \sum_{G \neq 0} \frac{exp\left(-\frac{|\boldsymbol{G}|^2}{4\alpha^2}\right)}{|\boldsymbol{G}|^2} \sum_i \sum_j \frac{Q_i Q_j}{4\pi\varepsilon_0} \cos\left\{\boldsymbol{G} \cdot \left(\boldsymbol{r}_i - \boldsymbol{r}_j\right)\right\} \tag{8.22}$$

Here $\boldsymbol{G}$ is a reciprocal lattice vectors. This summation can be done for one half of the vectors, because terms (h, k, l) and $(-h,-k,-l)$ in the reciprocal space have the same values. The Gaussian distribution introduced guarantees the convergence of the summation in the reciprocal lattice vectors.

The Third Term of the Ewald Summation, φ_{self}

In the reciprocal term, φ_{self}, extra electrostatic potential by the ion "i" having a Gaussian distribution is included and the following term should be subtracted off.

$$\varphi_{self} = \sum_i \frac{Q_i Q_i}{4\pi\varepsilon_0} \frac{\alpha}{\sqrt{\pi}}, \tag{8.23}$$

Setting of the Ewald Method

The error in the Ewald summation is determined by the choice of α and L values. The optimal choice can be done by several methods [96]. For example, when $L \sim 20$ Å is used, 125 vectors are necessary to carried out the simulation with a tolerance of 10^{-5} in the energy of the Ewald sum. In several software of MD, the combination can be selected automatically or set by the choice of a value of tolerance.

The reciprocal lattice term has the factor $1/|\mathbf{G}|^2$, which diverges at $\mathbf{G} = 0$. To avoid the divergence of the second term, $\mathbf{G} = 0$ is omitted and this procedure is justified by the condition of the charge neutrality of the system. Thereby the method does not hold exactly in system with defects. It may be better to consider the charge redistribution to fulfill the neutrality in such a case, or to use other method such as the multipole expansion.

8.2.5.2 Particle Mesh Ewald (PME) and Particle-Particle-Particle-Mesh (P^3M) Ewald Method

Instead of the Ewald method with the $O(N^{3/2})$ character [90, 92], particle-particle-particle-mesh (P^3M) method was developed as the $O(N)$ method [93, 94]. In the case of P^3M, interaction of short length is treated by particle-particle, while the long ranged interaction was treated by particle-mesh interaction. To obtain the $O(N)$

condition in this method, real space region is more limited than the optimized one for the Ewald summation, and the calculation times of real space and reciprocal space are set to be comparable. Particle-Mesh Ewald [95], which is an $O(N\log N)$ method, is a special case of P^3M method, although it was independently developed.

8.2.6 Multipole Expansion and Tree Method

Usually, the force from particles located at the long distance is weak. One of the possible ways to reduce the calculation cost is to handle some numbers of particles together. The group can be represented by the sum of multi-poles. To distinguish the distant particles from the particles close by, the "tree method" has been proposed. The "multipole method" with a multipole expansion is typically used with the "tree method" or "hierarchy tree method" [97–99, 100], which can separate groups by a distance effectively, without calculating the distance among particles. For example, the "Quad tree code" (for 2D case) repeats the division of the system into four until each region contains less than a certain number of particles (0 or 1) (see Fig. 8.2). "Oct tree code" is for the case of 3D.

If both the particles acting and those being affected on are treated as groups, it is called "fast multipole method (FMM)" and is shown to be an $O(N)$ method. The method using multipoles is effective for extremely large system and also for the system without a periodic boundary, since one can consider the force acting from the sub-regions or grids (cells) of the system instead of individual particles. Now we considered a case of interaction from M particles in a sub-region to the outer point

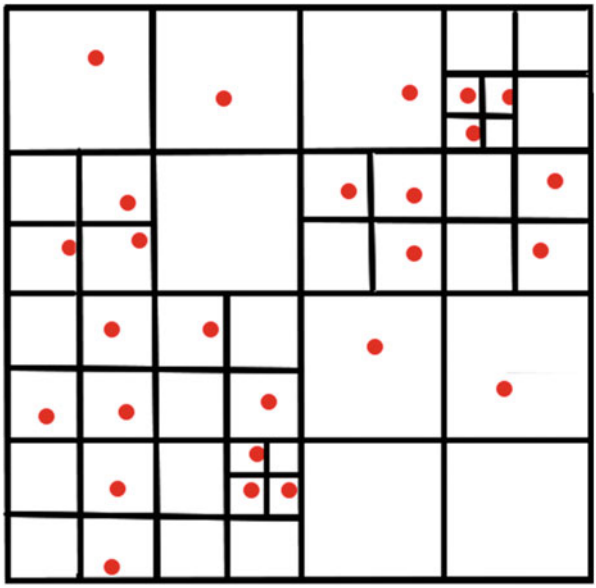

Fig. 8.2 Schematic description of the "Quadtree code" for the 2D structure, which can separate group of particles without calculating the distance

P to understand the merit of using multipoles. Here the center of the cell is represented as $\mathbf{r}_c$ and the relative positions of particles k ($k = 1, 2$----M) to the center are taken as $\mathbf{r}_k$. A Coulombic potential formed at the point P is represented as,

$$\varphi_C(\boldsymbol{r}) = \sum\nolimits_{k=1}^{M} \varphi_C(|\boldsymbol{r}_{k-}\boldsymbol{R}|) = \sum\nolimits_{k=1}^{M} \frac{q_k}{|\boldsymbol{r}_{k-}\boldsymbol{R}|}, \tag{8.24}$$

The vector $\boldsymbol{R}$ is a relative position of P from the center of the sub-region and q_k is a point charge. At the arbitrary chosen position $\boldsymbol{r}$, the potential function can be approximately represented as follows.

$$\varphi_C(\boldsymbol{r}) = \frac{Z}{R} + \frac{\mu_\alpha R_\alpha}{R^3} + \frac{Q_{\alpha\beta} R_\alpha R_\beta}{R^5} + \cdots, \tag{8.25}$$

In the right hand side of the equation, Z is a sum of charge within a grid, $Z = \sum_k q_k$, μ_α is a dipole moment, $\mu_\alpha = \sum_k q_k \boldsymbol{r}_{k\alpha}$, and $Q_{\alpha\beta}$. is a quadrupole, given by $Q_{\alpha\beta} = \sum_k q_k \frac{m}{2} \left\{ \left(3\boldsymbol{r}_{k\alpha} - \delta_{\alpha\beta} \mathbf{r}_k^2 \right) \right\}$.

The strength of the charge decreases with $1/r$, while that of dipolar decreases ~$1/r^2$ and so on. In this expression, $\mu_\alpha R_\alpha$ is for a sum of $\alpha = x,y,z$; while $\boldsymbol{r}_{k\alpha}$ is a $\alpha = x,y,z$ component of vector $\mathbf{r}_k$. This treatment, which dividing the basic cell into sub-regions, is also useful for the parallel computing.

8.2.7 General Description of the Multipole Expansion

One can represent any charge distribution by using multipole expansion and this kind of treatment is also applicable for $1/r^m$ type potentials besides the Coulombic term. Therefore, more general treatment using spherical harmonics [101] will be useful in some situations. Outside of the ionic system, one assumes that the electrostatic potential ϕ(r) satisfies the following Laplace equation,

$$\nabla^2 \phi(r) = 0 \tag{8.26}$$

Under the condition that "at the long r limit, φ(r) becomes 0", the solution of the equation can be expanded as follows.

$$\phi(r) = \frac{1}{4\pi\varepsilon_0} \sum_{l=0}^{\infty} \sum_{m=-l}^{l} \frac{4\pi}{2l+1} q_{lm} \frac{Y_{lm}(\theta, \varphi)}{r^{l+1}} \tag{8.27}$$

Here the terms $Y_{lm}(\theta, \varphi)$ are the spherical harmonics (i.e., the angular part of the solution). One may be familiar with the graphical representation of the spherical

harmonics, because it is frequently used to represent the shape of orbital of electrons such as π-orbitals or *d*-orbitals. For example, one can see the shape of the spherical harmonics. [For example, see Wolfram Demonstration Project, Spherical Harmonics, http://demonstrations.wolfram.com/SphericalHarmonics/ (The address was confirmed to be valid on 14th Feb., 2016.)]. The function is also used to characterize structures of bond ordering, local or intermediate structures in super-cooled liquids, glasses or crystals [66, 102].

The Eq. (8.27) as well as (8.25) is called a multipole expansion of the electrostatic potentials, where the q_{lm} is a multipole moment, which is related to the distribution of the density ρ(*x*') as shown in,

$$q_{lm} = \int_{\Omega} Y_{lm}^{*}(\theta', \phi') r'^{l} \rho(r') dr'. \tag{8.28}$$

When the total charge is denoted by q and the dipole moment is denoted by $p = \int_{\Omega} x' \rho(x') dx'$, then the following relations are obtained.

$$q_{00} = \frac{1}{\sqrt{4\pi}} \int_{\Omega} \rho(x') dx' = \frac{q}{\sqrt{4\pi}} \tag{8.29}$$

$$q_{l,\pm 1} = \mp \sqrt{\frac{3}{8\pi}} \int_{\Omega} (x' \mp iy') \rho(x') dx = \mp \sqrt{\frac{3}{8\pi}} (p_x \mp i p_y) \tag{8.30}$$

$$q_{l0} = \sqrt{\frac{3}{4\pi}} \int_{\Omega} z' \rho(x') dx = \sqrt{\frac{3}{4\pi}} p_z \tag{8.31}$$

Here $l = 0$ is for point charge ($m = 0$), $l = 1$ is for dipole moment($m = -1, 0, 1$), $l = 2$ corresponds to quadrupole ($m = -2, -1, 0, 1, 2$), and $l = 3$ corresponds to 8-pole moment and so on. The concept of multipoles is useful not only for calculations of Coulombic terms during simulation but also for understanding the force affecting the ions.

8.2.8 *Multipoles as an Origin of Nearly Constant Loss (NCL) of Caged Ion Dynamics*

Usually, interaction of neighboring ions or atoms is directly summed up in MD; however, it is possible to consider the multipole expansion of interaction from surrounding particles as a cage. Let us consider the cage formed by oxygen atoms around Li ions as in silicate or related systems. Each Li ion is trapped inside the cage formed by oxygen atoms and rocked. Instead of direct interaction between Li

ion and oxygen atoms, the same potential (Coulombic term) can be represented as the sum of multipoles up to l_{max}. Here the accuracy becomes better if the l_{max} is larger, where the first term (charge-charge interaction) is considered for the center of mass position of oxygen atoms. As already mentioned, contribution of the dipole ($\sim 1/r^2$) decays faster than that of point charge ($\sim 1/r$), while contribution of quadrupole ($\sim 1/r^3$) decays faster than that of the dipole. Thus the potential of the cage, consisting sum of these terms, is anharmonic. In previous chapters, we have shown that anharmonic potential acting on the ions causes caging of the ions at short times, and observed experimentally in susceptibility as the nearly constant loss (NCL).

Here we do not exclude the contribution of repulsive terms, and note that representation by the multipoles is also applicable to the repulsive part. Represented by the multipoles and their time dependence, the anharmonic potential is effective in caging the ions, and the loss from motion of ions confined within the cages is manifested as the NCL in susceptibility (See Sects. 4.5, 4.7 and 9.4.2.). Previously, Dieterich and Maass considered the asymmetric double well potential, and/or random dipole interaction as an origin of NCL [103]. If the total charge in the caging region is 0, then the main term will be dipole (if it is not 0). Although this might be a good approximation in some cases, further terms will be necessary to represent the situation more precisely. In the ionic structures, alternative oscillation of positive and negative charges are observed at longer length scales than neighboring distance and this means that the charge neutrality does not hold within the neighboring distance. When the total sum of q is not 0, point charge term cannot be neglected. Actually, we have previously shown that the motion of Li ions in the lithium metasilicate system is well correlated with the motion of center of mass position of polyhedral formed by caging oxygen atoms [3, 68]. Contribution of further terms also will not be negligible especially in the short distance region. We also note that the cage is moving in NCL region and therefore its motion is characterized as dynamic anharmonicity as discussed in Sect. 9.5.2.

Generally, the nature of cages is also related to the problem of glass transition [104, 105], because the rigidity or softness of the cages determines the motion of ions, atoms, or molecules trapped within [106].

8.2.9 Treatment of Rotational Motion

8.2.9.1 Euler Angles

When ions or molecules of the system have internal structures, methods to include consideration of rotational motion are necessary in MD simulations. In such cases, motions of ion or molecule are regarded as a combination of translational motion of the center of mass position, P, and rotational motion around it. The rotational motion is represented by the Euler's equations [91, 107] named after Leonhard Euler using Euler angles, where the coordinates (P-$\widetilde{x}\widetilde{y}\widetilde{z}$) fixed on body, centered at P are used.

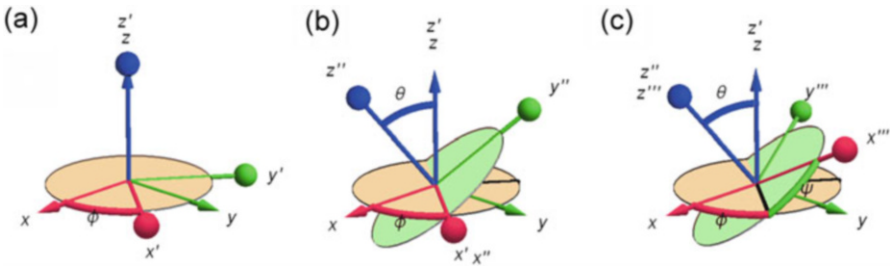

Fig. 8.3 Orientation of rigid body is represented by the Euler angles, ϕ, θ and ψ. Definition of Euler angles by Goldstein is shown here. The rotation is measured in counterclockwise direction. In this example, ϕ, θ and ψ used are 0.92, 0.67 and 0.87, respectively

The coordinate (P-$\widetilde{x}\widetilde{y}\widetilde{z}$) is transformed from the space coordinate (O-xyz) as follows, where P and O are overlapped. There are several notations and definitions for the treatment of angles. Here we used ones by Goldstein [108]. In these procedures, the rotation is counterclockwise and is in three steps as shown in Fig. 8.3.

1. The coordinate (O-xyz) is rotated around z axis with angle φ (see Fig. 8.3a).
2. A resultant coordinate (O-x′y′z′) is rotated around x′ axis with angle θ (see Fig. 8.3b).
3. A resultant coordinate (O-x″y″z″) is rotated around z″ axis with angle ψ (see Fig. 8.3c). The final coordinate after the rotations is O-x‴y‴z‴ (=P-$\widetilde{x}\widetilde{y}\widetilde{z}$) in Fig. 8.3c.

Rotational transformation of the vector **A** in (O-xyz) coordinate to **B** in P-$\widetilde{x}\widetilde{y}\widetilde{z}$ coordinate is represented as follows.

$$\mathbf{B} = \mathbf{AR}. \tag{8.32}$$

Here **R** is a transformation matrix shown below.

$$\begin{aligned}\mathbf{R} &= \mathbf{R}_{\varphi}\mathbf{R}_{\theta}\mathbf{R}_{\psi} \\ &= \begin{pmatrix} \cos\psi\cos\phi - \cos\theta\sin\phi\sin\psi & \cos\psi\sin\phi + \cos\theta\cos\phi\sin\psi & \sin\psi\sin\theta \\ -\sin\psi\cos\phi - \cos\theta\sin\phi\cos\psi & -\sin\psi\sin\phi + \cos\theta\cos\phi\cos\psi & \cos\psi\sin\theta \\ \sin\theta\sin\phi & -\sin\theta\cos\varphi & \cos\theta \end{pmatrix},\end{aligned} \tag{8.33}$$

where $\mathbf{R}_{\phi} = \begin{pmatrix} \cos\phi & \sin\phi & 0 \\ -\sin\phi & \cos\phi & 0 \\ 0 & 0 & 1 \end{pmatrix}$

$$\mathbf{R}_\theta = \begin{pmatrix} 1 & 0 & 0 \\ 0 & \cos\phi & \sin\phi \\ 0 & -\sin\phi & \cos\phi \end{pmatrix}$$

And $\mathbf{R}_\psi = \begin{pmatrix} \cos\psi & \sin\psi & 0 \\ -\sin\psi & \cos\psi & 0 \\ 0 & 0 & 1 \end{pmatrix}$.

A transformation from **B** to **A** is by using transpose matrix,

$$\mathbf{A} = {}^t\mathbf{R}\mathbf{B} \tag{8.34}$$

8.2.9.2 Euler's Equations

Kinetic energy, K_R of the rotational motion of rigid body is represented as follows by using the inertia tensor.

$$K_R = \frac{1}{2}\Big[I_{xx}\omega_{\tilde{x}}{}^2 + I_{xy}\omega_{\tilde{x}}\omega_{\tilde{y}} + I_{xz}\omega_{\tilde{x}}\omega_{\tilde{z}} + I_{yz}\omega_{\tilde{y}}\omega_{\tilde{x}} + I_{yy}\omega_{\tilde{y}}^2 + I_{yz}\omega_{\tilde{z}} + I_{zx}\omega z\omega_{\tilde{x}} + I_{zy}\omega_{\tilde{z}}\omega_{\tilde{y}} + I_{zz}\omega_{\tilde{z}}^2\Big]. \tag{8.35}$$

If the P-$\widetilde{x}\widetilde{y}\widetilde{z}$ is chosen to be coincident with the principal axes of inertia, inertia tensor is simplified to be represented by the diagonal elements, and time dependence of the angular momentum can be represented by the Euler's equations.

Time derivative of the angular momentum $\mathbf{L}_\mathrm{R}$ in O-xyz coordinate is,

$$\frac{d\mathbf{L}_R}{dt} = \mathbf{T}_R, \tag{8.36}$$

here $\mathbf{T}_R$ is torque vector and total angular momentum of the rigid body (molecule, ion, etc.) consists of N particles can be obtained by $\mathbf{L}_R = \sum_{i=1,N} m_i\mathbf{r}_i \times d\mathbf{r}_i/dt$.

While the angular momentum $\mathbf{L}_\mathrm{P}$ in the P-$\widetilde{x}\widetilde{y}\widetilde{z}$ coordinate is represented by

$$\mathbf{L}_P = \begin{pmatrix} L_{P\widetilde{x}} \\ L_{P\widetilde{y}} \\ L_{P\widetilde{z}} \end{pmatrix} = \begin{pmatrix} I_1 & 0 & 0 \\ 0 & I_2 & 0 \\ 0 & 0 & I_3 \end{pmatrix} \begin{pmatrix} \omega_{P\widetilde{x}} \\ \omega_{P\widetilde{y}} \\ \omega_{P\widetilde{z}} \end{pmatrix} = \begin{pmatrix} I_1\omega_{P\widetilde{x}} \\ I_2\omega_{P\widetilde{y}} \\ I_3\omega_{P\widetilde{z}} \end{pmatrix}, \tag{8.37}$$

where I_1, I_2, I_3 are the components of the principal moment of inertia in the P-$\widetilde{x}\widetilde{y}\widetilde{z}$ coordinate and $\omega_{P\widetilde{x}}$, $\omega_{P\widetilde{y}}$ and $\omega_{P\widetilde{z}}$ are the components of angular velocity about these principal axes.

Euler's equations can be derived from the transformation of time derivative of angular momentum $d\mathbf{L}_\mathrm{R}/dt$ in O-xyz coordinate to that ($d\mathbf{L}_\mathrm{P}/dt$) in P-$\widetilde{x}\widetilde{y}\widetilde{z}$ coordinate,

$$\frac{d\mathbf{L}_P}{dt}(in\ \ P-\widetilde{x}\widetilde{y}\widetilde{z}\ \text{coordinate})\ =\frac{d\mathbf{L}_P}{dt}\big(in\ \ O-xyz\ \text{coordinate}\big)+\omega\times\mathbf{L}_P. \quad (8.38)$$

Taking each component along principal axis of Eq. (8.38) for left hand side, Euler's equations are given as follows.

$$I_1\frac{d\omega_{P\widetilde{x}}}{dt}-\omega_{P\widetilde{y}}\omega_{P\widetilde{z}}(I_2-I_3)=\mathbf{T}_{P\widetilde{x}} \quad (8.39a)$$

$$I_2\frac{d\omega_{P\widetilde{y}}}{dt}-\omega_{P\widetilde{z}}\omega_{P\widetilde{x}}(I_3-I_1)=\mathbf{T}_{P\widetilde{y}} \quad (8.39b)$$

$$I_3\frac{d\omega_{P\widetilde{z}}}{dt}-\omega_{P\widetilde{x}}\omega_{P\widetilde{y}}(I_1-I_2)=\mathbf{T}_{P\widetilde{z}} \quad (8.39c)$$

8.2.9.3 Relation Between Angular Velocity and Euler Angles

The derivatives of angles $\dot{\varphi}$, $\dot{\phi}$ and $\dot{\theta}$, are z′, x″ and z‴ components of angular velocity vectors ω'_{ϕ}, ω''_{θ} and ω'''_{ψ} in the P-x′y′z′, P-x″y″z″ and P-x‴y‴z‴(=P-$\widetilde{x}\widetilde{y}\widetilde{z}$) coordinates, respectively. Therefore, the following relation holds.

$$\boldsymbol{\omega}=\mathbf{R}_{\phi}\mathbf{R}_{\theta}\omega'_{\phi}+\mathbf{R}_{\phi}\omega''_{\theta}+\omega'''_{\psi} \quad (8.40)$$

By solving Eq. (8.40) for each derivative of angle, the following results

$$\begin{aligned}\dot{\theta}&=\omega_{\tilde{x}}\cos\psi-\omega_{\tilde{y}}\sin\psi,\\ \dot{\phi}&=\frac{1}{\sin\theta}\big(\omega_{\tilde{x}}\sin\psi+\omega_{\tilde{y}}\cos\psi\big),\\ \dot{\psi}&=\omega_{\tilde{z}}-\frac{\cos\theta}{\sin\theta}\big(\omega_{\tilde{x}}\sin\psi+\omega_{\tilde{y}}\cos\psi\big),\end{aligned} \quad (8.41)$$

are obtained.

8.2.9.4 Relation Between Quaternion and Euler Angles

Since the temporal derivative of the Eulerian angle contains singular point (the term 1/sin θ in Eq. (8.41) becomes ∞ and $-\infty$, at 0 and π, respectively.), the Quaternion parameters [109] are used to avoid it. Quaternion parameters (ξ,η,ζ,χ) are connected to Goldstein's Euler angles θ,ψ,ϕ as follows.

$$\xi=\sin(\theta/2)\bullet\sin\big((\psi-\varphi)/2\big)$$

$$\begin{aligned}\eta &= \sin(\theta/2) \bullet \cos\big((\psi - \phi)/2\big)\\ \zeta &= \cos(\theta/2) \bullet \sin\big((\psi + \phi)/2\big)\\ \chi &= \cos(\theta/2) \bullet \cos\big((\psi + \phi)/2\big)\end{aligned} \tag{8.42}$$

Because of the relation, $\xi^2 + \eta^2 + \zeta^2 + \chi^2 = 1$, these four parameters are not independent and therefore, the degree of freedom does not change with the transformation.

8.2.10 Ensembles Used for MD Simulations

Several ensembles are used in MD simulations including extended ones. Some typically used ensembles are introduced here.

8.2.10.1 Constant Energy Condition

Constant number of atoms, volume and energy (NVE) ensemble (micro-canonical ensemble) is achieved without modification of system, while extended ensemble such as NPT, NVT (P: pressure, T: temperature) requires additional parameters to control the pressure and/or temperatures.

8.2.10.2 Constant Pressure Condition (Andersen Method)

Andersen [110] developed the method to control the pressure by introducing the wall (a three dimensional piston) in the MD cell. This treatment is explained here for the case of soft-core (SC) model.

The Hamiltonian of the SC system interacting pair-wise force is

$$H(p, r) = \sum_j p_j^2/2m + \sum_{i<j} \varepsilon\big(\sigma/r_{ij}\big)^n \equiv K + U, \tag{8.43}$$

where the m and σ are the mass and a size parameter of the particle, respectively. Hamiltonian in the extended system can be written as follows,

$$H(\mathbf{s}, \boldsymbol{\pi}, V, \Pi) = \sum_i (\boldsymbol{\pi}_i \bullet \boldsymbol{\pi}_i)/\left(2mV^{2/3}\right) + U\left(\left[V^{1/3}\mathbf{s}\right]\right) + \frac{1}{2M}\Pi^2 + P_{ex}V, \tag{8.44}$$

where $\mathbf{s}\big(= s_{ix}, s_{iy}, s_{iz}\big)$, $\boldsymbol{\pi}_i\left(= \frac{\partial L}{\partial s_i^{\bullet}}\right)$ and $\Pi\left(= \frac{\partial L}{\partial \dot{V}} = M\dot{V}\right)$ are normalized ($\mathbf{r}_i = L\mathbf{s}_i$) coordinates, momentum of particle i and momentum of the wall respectively, and

$P_{ex}V$ is a potential energy by the wall. Here we consider the isotropic system with $L = V^{1/3}$. The system is conservative.

In the equilibrated system with a constant pressure, the term $\frac{1}{2M}\Pi^2$ becomes negligibly small, where M has the dimension of [mass][(length)$^{-4}$]. Then one can use the reduced mass M' which is given by the relations [91]

$$M' = M\sigma^4/m. \tag{8.45}$$

The system under the constant pressure condition is controlled by the difference of external pressure and internal pressure.

From Eq. (8.9), equations of motions are obtained as follows.

$$\frac{d\mathbf{s}_i}{dt} = \frac{\partial H}{\partial \boldsymbol{\pi}_i} = \frac{1}{m_i V^{2/3}}\boldsymbol{\pi}_i \tag{8.46a}$$

$$\frac{d\boldsymbol{\pi}_i}{dt} = -\frac{\partial H}{\partial \mathbf{s}_i} = \frac{\partial U}{\partial \mathbf{s}_i}, i = 1, 2, 3, \ldots, N \tag{8.46b}$$

$$\frac{dV}{dt} = \frac{\partial H}{\partial \Pi} = \frac{\Pi}{M}, \tag{8.46c}$$

$$\frac{d\Pi}{dt} = -\frac{\partial H}{\partial V} = \frac{\Pi}{M} = \frac{1}{3V}\left(V^{-2/3}\sum_i \frac{\dot{\boldsymbol{\pi}}_i \bullet \dot{\boldsymbol{\pi}}_i}{m_i} - V^{1/3}\frac{\partial U}{\partial\left(V^{1/3}\right)}\right) - P_{ex} \tag{8.46d}$$

These equations of motion for the scaled system are solved numerically to give the time development of coordinates and momenta.

The correspondence between the scaled system and the original system is taken into account through the following relations.

$$\mathbf{r}_i = L\mathbf{s}_i \tag{8.47}$$

$$\mathbf{p}_i = L^{-1}\boldsymbol{\pi}_i. \tag{8.48}$$

$$\frac{d\mathbf{r}_i}{dt} = \frac{\mathbf{p}_i}{m} + \frac{\mathbf{r}_i}{3V}\frac{dV}{dt}, \tag{8.49a}$$

$$\frac{d\mathbf{p}_i}{dt} = \frac{\partial U}{d\mathbf{r}_i} - \frac{\mathbf{P}_i}{3V}\frac{dV}{dt}, \tag{8.49b}$$

$$\frac{dV}{dt} = \frac{\Pi}{M}, \tag{8.49c}$$

$$\frac{d\Pi}{dt} = \frac{1}{3V}\left(\sum_i \frac{\mathbf{p}_i{}^2}{m_i} - \sum_{i=1}^{N-1}\sum_{j>i}^{N}\frac{\phi(r_{ij})}{dr_{ij}}\frac{\mathbf{r}_{ij}\bullet\mathbf{r}_{ij}}{r_{ij}}\right) - P_{ex} \tag{8.49d}$$

The first term in Eq. (8.49d) represents the instantaneous internal pressure. When the internal pressure equals to the external pressure P_{ex}, $\frac{d\Pi}{dt} = 0$ and then the system volume becomes constant. In other cases, the instantaneous pressure (and volume)

fluctuates around the P_{ex} set in the simulations. This situation can be regarded as the thermally equilibrated state, with the use of a suitable M. Time average of any function (which corresponds to NVH ensemble), F, can be calculated from the trajectories obtained by the Eq. (49).

8.2.10.3 Constant Temperature Condition (Nosé Method)

For controlling temperature, thermostat using a fictive time with a new degree of freedom, (s, p_s), is introduced by Nosé [86, 111–114]. Here, s and p_s correspond to the coordinate and its canonically conjugate variable, momentum, of the new degree of freedom having mass represented by Q. The coordinate and its canonically conjugate variable, momentum, in the extended (fictive) system are represented by $\mathbf{r}'$ and $\mathbf{p}'$, respectively.

The Hamiltonian of the extended system is defined by

$$H(\mathbf{p}', \mathbf{r}', p_s, s) = \sum_i \left(\mathbf{p}_i'^2/\left(2ms^2\right) + U(\mathbf{r}') + \frac{{p_s}^2}{2Q} + gk_BT\ln s, \tag{8.50}$$

where g is a parameter used to represent the degree of freedom.

In this case, T is a parameter to give the targeted value of the temperature, and Nosé has proved that the microcanonical ensemble of the extended system corresponds to the canonical (NVT) ensemble in the real system if one choose $g = 3N + 1$.

The values in the real and extended systems are assumed to be connected by

$$\mathbf{r}_i = \mathbf{r}_i', \quad \mathbf{p}_i = \frac{\mathbf{p}_i'}{s}, \quad t = \int^t \frac{dt'}{s}, dt = \frac{dt'}{s}$$

The last two equations represent the relation between the time in the extended system, t', and that in the real system, t.

Then the velocity of these systems are connected by,

$$\frac{d\mathbf{r}_i}{dt} = \frac{d\mathbf{r}_i}{dt'}\frac{dt'}{dt} = s\frac{d\mathbf{r}_i'}{dt'}. \tag{8.51}$$

The Hamilton's canonical equations for the extended system are derived from (Eq. 46) are given by,

$$\frac{d\mathbf{r}_i'}{dt'} = \frac{\partial H}{\partial \mathbf{p}_i'} = \frac{\mathbf{p}_i'}{ms^2}, \tag{8.52a}$$

$$\frac{d\mathbf{p}_i'}{dt'} = -\frac{\partial H}{\partial \mathbf{r}_i'} = -\frac{\partial U}{\partial \mathbf{r}_i'}, \tag{8.52b}$$

$$\frac{ds}{dt'} = -\frac{\partial H}{\partial p_s} = \frac{p_s}{Q}, \tag{8.52c}$$

$$\frac{dp_s}{dt'} = -\frac{\partial H}{\partial s} = -\frac{\partial W(s)}{\partial s} = \sum_i \frac{\mathbf{p}_i'^2}{ms^3} - \frac{gk_BT}{s}. \tag{8.52d}$$

In Eq. (8.52d), $W(s)$ $\left(= \frac{K}{s^2} + gk_BT\ln s \text{ with } K = \sum_i \frac{\mathbf{p}_i'^2}{2m} \right)$ corresponds to the potential energy relating to the giving and receiving the heat.

From Eq. (8.50), the equation of motion in the real system is derived as [91, 111],

$$\frac{d\mathbf{r}_i}{dt} = \frac{\mathbf{p}_i}{m}, \tag{8.53a}$$

$$\frac{d\mathbf{p}_i}{dt} = -\frac{\partial U}{\partial \mathbf{r}_i} - p_s\mathbf{p}_i/Q, \tag{8.53b}$$

$$\frac{ds}{dt} = s\frac{ds}{dt'} = sp_s/Q, \tag{8.53c}$$

$$\frac{dp_s}{dt} = s\frac{dp_s}{dt'} = \sum_i \frac{\mathbf{p}_i^2}{m_i} - gk_BT. \tag{8.53d}$$

The equations of motion in the real system are slightly modified to

$$\frac{d\mathbf{r}_i}{dt} = \frac{\mathbf{p}_i}{m}, \tag{8.53a'}$$

$$\frac{d\mathbf{p}_i}{dt} = -\frac{\partial U}{\partial \mathbf{r}_i} - \zeta\mathbf{p}_i, \tag{8.53b'}$$

$$\frac{d\zeta}{dt} = \frac{2}{Q}\left[\sum_i \frac{\mathbf{p}^2{}_i}{2m} - \frac{gk_BT}{2}\right], \tag{8.53c'}$$

where $ds/dt = s\zeta$. Under the conditions, $x_s = \ln s$ and $\zeta = \dot{x}_s = \frac{p_s}{Q}$, these equations are equivalent to Eqs. (8.53a–8.53d).

This form of the thermostat, which is by eliminating s, is called the Nosé-Hoover thermostat [112], and it can reproduce the canonical distribution in the coordinate space.

Because the variable s for the scaling of time of whole system is eliminated, the friction coefficient ζ can be defined for each substructure of the system and it is useful for the controlling temperatures in complex systems. Sampling of data intervals used in a virtual system in the Nosé algorithm corresponds to the unequal sampling of that in the real space. The Nosé-Hoover algorithm also removes this difficulty, although the resulting system is not Hamiltonian. Recently, the Nosé-Poincaré method [86, 114] was introduced to solve this problem.

8.2.10.4 Combination of Conditions

Nosé generalized the work to include both thermostat and barostat. Nowadays, many kinds of extended ensembles are introduced and used [87, 91, 115].

In Sect. 8.5.3, our attention will be focused on the problem of the choice of ensembles to study structures and dynamics in super-cooled liquids or glasses including non-equilibrium situations. Some other problems concerned with the system showing slow dynamics will be also discussed there. Dynamics in crystals are also slow process and similar treatment seems to be required.

8.2.11 Parrinello-Rahman Methods

It is useful for the simulation of the crystal and its transformation, additional degree of freedom is taken into account. In the Parrinello-Rahman (and Parrinello-Rahman-Ray) methods [116–118], angles as well as axis lengths in the basic cell (with parallelepiped structure) can be changed during the MD runs. Practically, it seems to work in several conditions after the equilibration, although it is known that the collapse of the parallelepiped structure occurs in some cases. It may be helpful to consider the geometrical degree of the freedom [119] of the basic cell of MD to treat this problem.

8.2.12 High Performance Computation

If one would like to treat large system and for long times in a straightforward manner, acceleration of the calculation is desired, as well as the developments of computer technology itself. Another possible way is to reduce the amount of calculation itself. Coarse-graining by several methods and scaling concepts are effective for estimation and prediction of long time behavior of the system, and may save the calculation times. Here we mention the means for accelerating the calculations.

8.2.12.1 Parallel Computing, Acceleration Boards, and Graphic Processing Unit (GPU)

In MD simulations, each particle moves by the sum of forces from other particles. This calculation is the most time consuming part for the simulations. Many particles can be treated by several kinds of parallel computing, using Message Passing Interface (MPI), graphic processing unit (GPU), *etc*. Several methods for parallel computing both by manipulating software and hardware can be applied.

The GRAPE (Gravity Pipe) board was developed for solving the 'Gravitational Many-Body Problem', where the common algorithm with molecular dynamics is used. Then, MDGRAPE [120] chip was designed for acceleration of MD simulation.

Recently, graphic processing unit (GPU) pioneered by NVIDIA in 2007 [http://www.nvidia.com/object/what-is-gpu-computing.html (The address was confirmed to be valid on 14th Feb. 2016).] is widely used for acceleration of computation including MD and is called GPGPU (General-purpose computing on graphics processing units) (see also Appendix 8). GPU boards named Tesla and/or GeForce are included in many computing systems, not only super-computers but also in personal computers. Because of its generality and relatively lower cost, the methodology is rapidly spreading. Such developments will make an MD simulation suitable for personal use in the near future. An example of coding for the main loop of MD by Fortran using Compute Unified Device Architecture (CUDA) is shown in the Appendix A.8.1.

There are several problems for each technology. Sometimes, heat released on the boards causes many problems such as instability of the system. Noises coming from the fan for cooling may cause another problem. Therefore, controlling the heat release is an important problem for using acceleration boards. If the board is occupied by a job in an exclusive manner, it will prevent the execution of parallel computing jobs. Parallel calculations are effective to use for large system but not necessarily being effective enough for long runs. This is because the MD run of slow dynamics is essentially sequential to cover the different time regions. Therefore the technology different from the parallel computation may be desirable. Parallel computing of completely independent runs (of different conditions) is one of the alternative approaches. "Array job" can be used in some systems for parameter survey.

8.2.12.2 Difference in Numerical Results Using Parallel Computations

If one uses the symplectic integrator, the drift of the energy can be avoided in the equilibrium system. Nevertheless, drift may occur due to different origins such as the overlaps of non-equilibrium relaxations and/or aging. When calculated values in parallel calculations are accumulated into one, resultant data will have larger numerical errors compared with calculation on the single machine. Besides these problems, in the case of slow dynamics in supercooled liquids or glasses, further caution seems to be required for the deterministic nature of the motion.

Ionics in the glassy state is dominated by jump motion of ions and it has intermittent and sporadic nature related to chaos. Consequently, each motion is quite sensitive for the small difference of the initial value. Each ionic motion tends to show the different trajectory by this. This situation occurs regardless of single precision or double precision of the calculation and therefore it is not a problem of the number of significant digits. It is not a problem of the quality of GPU itself as well, although it occurs when the calculation is just moved from CPU to GPU.

This is because similar situation also occurs just by changing the order of the calculation within a Do loop [The view discussed here is obtained by the assistance of the staffs of the project of acceleration of the program using GPU in the Global Scientific Information and Computing Center in Tokyo Institute of Technology. Here we appreciate it]. Sometimes one needs extremely long time runs for calculation of properties such as transport coefficients and their fluctuations, and one may have to worry about the propagation of errors during the run. Fortunately, the dynamic properties of long time, such as transport coefficients, tend to converge to certain values during a long run (for example, diffusion coefficient of ionic motion converges within 10 ns runs at 800 K in lithium disilicate) and this is also represented by using the local expansion rate [121], which can be a measure of the propagation of the error in non-linear dynamics [122, 123] (see also Sect. 8.4.2). It means that the short time fluctuation of motions does not affect the structure of the attracter for the long time dynamics. In other words, characteristics of the ion channels are not changed by the local motion in the caging region. In our opinion, the short time discrepancy does not necessarily affect the long time behavior of the mean dynamics and that is why we can use a long time run of MD simulations for the calculation of transport properties. Of course, each researcher has responsibility to check it for the result of MD runs in each system when parallel computation and/or long runs are used.

8.2.12.3 Perspective of Computational Technology in MD Simulations

During a long run of MD, one may encounter the situation of run being stopped by the problem of the machine or supply of electricity. To avoid such troubles, further developments for acceleration of long time runs will be helpful. One may also encounter the problem of coding in calculations for adjusting available resources. Although some compilers have an option for parallel computing, still it requires some modification of the code for efficient treatment. When a new hardware is developed, a new coding might be necessary. To improve the performance, developments of machine independent coding seem to be desirable. Recent development of "Xeon Phi co-processor" by Intel seems to show one of the promising ways for this direction, because it does not require the special coding.

8.3 Physical Quantity and Properties Obtained from MD Simulations

In typical classical MD simulations, input of the MD simulations is the "potential parameters" and the output is essentially the "time series of coordinates of particles (and velocities)", that is the "trajectories". Typical input files in the MD simulations of glasses contain the following items:

1. Setting of potential parameters and functions,
2. Setting of ensemble (NPT, NVE, etc.).
3. Preparation of initial configuration (and velocity) (system size).
4. Setting of runs (step time and steps for equilibration and those for analysis)

In the case of study of glasses or glass transition, cooling schedule is also required.

In typical output files, fundamental information such as temperature, energies, pressure, pair correlation functions are included in most of MD programs for checking the data and/or further treatment.

From the trajectories, further analyses can be done. Available information is concerned with the structures, dynamics and thermodynamics. Researcher can define any functions to obtain specific information suitable for their purpose. Visualization of the structures, motions, vectors is also useful. Furthermore, potential functions or parameters can be artificially modified if necessary. For example, mass, ionic size, and functional forms can be changed to examine the effects of each factor. These methods are useful to separate possible mechanisms responsible for the problem treated, and to check the results or prediction from models or theories. The model of the system can be tuned up for desired properties and hence MD simulations are applicable for material designs. In this sense, MD simulations are a tool of experimental investigations as well as of theoretical treatment. Some typical functions or properties obtained from MD are summarized in the next subsections. We hope that from the example of the research on silicate systems and ionic liquids in Chaps. 9–11, readers can have a good idea of how to use MD simulations.

8.3.1 Structural Properties

8.3.1.1 Pair Correlation Function: *g*(*r*)

Liquids have homogeneous structure at longer length scales and characteristics of them can be well represented by the pair correlation function [87, 91], where the structure is represented by a function of r only. This can be also used for characterizing super-cooled liquids and glasses, although further terms might be required in some circumstances.

Pair correlation function among different kind of particles i and j is obtained by

$$g_{ij}(r) = \frac{V}{N_i \bullet N_j} \left\langle \sum_{i=1}^{N_i} \frac{n_i(r - \Delta r/2, r + \Delta r/2)}{4\pi r^2 \Delta r} \right\rangle, \tag{8.54}$$

where V is a volume of the system, N_i and N_j are the number of the species i and j and $n_i(r - \Delta r/2, r + \Delta r/2)$ is the number of j particles within the shell with width Δr at distance r from particle i. The term $4\pi r^2$ is for the surface area of the sphere.

When the species i and j are the same one, the function is,

$$g_{ii}(r) = \frac{V}{N_i \bullet (N_i - 1)} \left\langle \sum_{i,=1}^{N_i} \frac{n_i(r - \Delta r/2, r + \Delta r/2)}{4\pi r^2 \Delta r} \right\rangle, \tag{8.55}$$

where now $n_i(r - \Delta r/2, r + \Delta r/2)$is the number of i particles within the shell with width Δr at distance r. Practically, it can be calculated during the MD run and it is useful to check the status of the calculation. In this case, distances among i and j particles appeared are not ordered and this may prevent the effective coding for parallel computation. A part using random access may be better to put it out of the loop of the calculation of force, if necessary. The $(N_i - 1)$ term is the number of surrounding particles, which does not include the central particle i.

For example, in the case of ionic liquids with internal structures, the function $g(r)$ for each pair can be determined for the center of mass position (or center of charges) of each ion. Alternative arrangement of cation and anion in ionic system tends to neutralize structure at a certain length scale. This behavior is regarded as screening in the strongly-coupled system such as NaCl [124, 125] and charge radial distribution in the following form is suggested.

$$q(r) = \frac{A}{r} \exp(-r/\lambda_D) \sin(2\pi r/d + \varphi), \tag{8.56}$$

where A/r is the amplitude, φ is the phase shift and d is the period of the oscillations.

In ionic structures, one can consider the charge distribution function $Q(r)$ and the density distribution function $G(r)$ defined by the following equations [124–127] by assuming that the charge is simply on the center of mass (or charge) position,

$$Q(r) = Q_+(r) + Q_-(r) = \{g_{++}(r) + g_{--}(r) - 2g_{+-}(r)\}e \tag{8.57}$$

$$G(r) = G_+(r) + G_-(r) = \{g_{++}(r) + g_{--}(r) + 2g_{+-}(r)\}/4 \tag{8.58}$$

The former is related to the structures of layers of charges (charge density wave, CDW), while the latter is related to structures of ionic positions regardless the charges (density wave, DW). Typical length scales for these functions are informative due to the difference of the main factors controlling them. These functions become 1 when the value becomes the mean density of species of the surrounding particles.

If the plots of $\ln|Q(r)r|$ against r have a straight line when the maxima of the peaks (envelopes) are connected, the characteristic length λ_Q, which corresponds to the Debye length for the screening of the Coulombic term in the simple dilute ionic systems, can be determined from the slope, $-1/\lambda_Q$. However, the values in dense ionic systems are not necessarily the same one as in a dilute system. The interaction observed is a renormalized one by the interactions from the other ions.

In the theory of liquids, the pair correlation function is fundamental to understand their structure [128, 129] and we note that the function can be obtained with good statistics in MD because it can be averaged in many steps.

8.3.1.2 Structure Factor and Intermediate Scattering Functions

Comparison of structures with experiments can be done through the structure factor $S(k)$. The function is a Fourier transform of $g(r)$ [128–132].

$$S(k) = 1 + 4\pi\rho \int_0^{r_{\max}} r^2 \{g(r) - 1\} \frac{\sin kr}{kr} dr. \tag{8.59}$$

Obtained by X-ray diffraction, the function is modified by the weight of atomic scattering factor, $f(k)$ [131, 132], while for neutron diffraction it is modified by scattering length, b. Details of the treatment of data is slightly different by different researchers. For example, the following form was used in some X-ray diffraction works, where $I(k) = S(k) - 1$.

$$kI(k) = \frac{\sum_i \sum_j x_i x_j f_i(k) f_j(k)}{\left\{\sum_i x_i f_i(k)\right\}^2} \times \int_0^{r_{max}} 4\pi\rho_0 \left\{g_{ij}(r) - 1\right\} \sin(kr) dr \tag{8.60}$$

Here ρ is the number density of the system and ρ_0 is the average of it.

For comparison of the structural details of glasses (such as Q_n where n is the number of bridging oxygen in the SiO_4 unit, the distributions or statistics of rings) from simulations with experiments, one should be careful to consider not only the cooling rate, but also the history of the system on the *PVT* phase-diagram (see Sect. 9.2). Otherwise, the results of the MD simulations might deviate from the experimental ones. This is because the partial structure (such as Q_n structure) has its specific partial volume [133, 134].

The formation of three dimensional networks is observable directly in MD simulations.

8.3.1.3 Running Coordination Numbers

To examine the coordination shells of other particles or solvent, the pair correlation function is accumulated as represented by the running coordination numbers, $N_{\text{coord}}(r)$. The function for the species j around species i is defined as follows.

$$N_{coord}(r) \equiv \rho_j \int_0^r 4\pi r^2 g(r) dr. \tag{8.61}$$

This function also can be calculated during the MD runs.

Coordination number is often defined by the cutoff values corresponding to the distance of the first minimum position of $g(r)$. The function also can be used to obtain the fractal dimension of the structures in different length scale regimes.

8.3.1.4 Angular Distribution Function

Distribution of angles in the structure can be examined by MD simulations. The angular correlation function may be defined by using the number of particles, dN, located between $\theta - d\theta/2$ and $\theta + d\theta/2$, within a certain distance r.

$$P(\theta) = CdN/\sin\theta \, d\theta. \tag{8.62}$$

C is a normalization constant so that the integration over 2π becomes 1.

When the data points are uniformly spreading, the number of points on the polar is smaller than that of points on the peripherals. The term $\sin\theta$ is used to take into account this situation. Namely, such correction is used, when the distribution in a three dimensional (3D) space is a target of the problem. The absence of the modification by the sine term is also found in literatures, such as the case when the frequency of the appearance of the angle (for example, that among bonding) is the problem to be examined.

8.3.2 Dynamic Properties

8.3.2.1 Mean Squared Displacement (MSD) and Diffusion Coefficient (D)

The Mean Squared Displacement (MSD) of species a is obtained by the expression [87, 91],

$$<r_a{}^2(t)> = \left\langle \left\{ \sum_{i=1}^{N_a} (r_{ai}(t) - r_{ai}(0))^2 \right\} / N_a \right\rangle. \tag{8.63}$$

Here the angled brackets represent the average for different initial times or independent runs.

Using a sequence of particle positions during a run of T_1 period, we prepared N arrays of data sequence with slightly shifted initial time t_0 values and the data for N arrays were averaged. Wide time window covering fluctuation of dynamics is

required in the case when dealing with heterogeneous dynamics. In the case of equilibrated system, it is the same as the ensemble average. However, in the case of non-ergodic system, it is not necessarily the same.

For each species, the MSD starts to become proportional to time t at times longer than t_{dif}. From the slope of the MSD at times longer than t_{dif}, the diffusion coefficients, D, can be obtained using the Einstein relation [135].

$$D = \frac{1}{6} \lim_{t \to \infty} \frac{d}{dt} < [r_i(t) - r_i(0)]^2 > . \tag{8.64}$$

The onset time of steady state diffusion, t_{dif}, is a characteristic and fundamental time of the dynamics. Here the denominator 6 is used for the case of diffusion in three dimensional systems.

In slow dynamics of super-cooled liquids near the glass transition regimes, quasi-diffusive regime, where the MSD is proportional to time, can be found before the fractional power law regime, if one closely examine the data (see Sect. 9.4.2 for details). Therefore, it is necessary to distinguish it from the true long term diffusive regime, particularly if the observation time is limited. If the system has hierarchy structures, diffusive regime is not be easily attained. For example, particles might be located in different domains with different sizes, when observation is started.

Diffusion coefficients can also be obtained from the velocity autocorrelation function.

$$D = \frac{1}{3} \int_0^\infty \langle \mathbf{v}(t) \bullet \mathbf{v}(0) \rangle. \tag{8.65}$$

This equation is known as the Kubo formula [136].

The function may seem to be converging at a short time (several ps) at a first glance even in glasses. However, this is not for a true diffusive regime. Thus, to ensure correct result for D, the times for the integration should be long enough to cover steady state diffusive motion.

8.3.2.2 Conductivity

Conductivity is connected with the complex frequency dependence of the ion dynamics and is related to the time dependence of the MSD by the relation [136, 137],

$$\sigma^*(\omega) = -\omega^2 \frac{Nq^2}{6H_R k_B T} \int_0^\infty < r^2(t) > e^{-i\omega t} dt, \tag{8.66}$$

where N is the number density of mobile ions, q the ion charge, k_{B} the Boltzmann constant, H_R the Haven ratio [138] and T the temperature.

In MD, the Haven ratio, $H_R = D_t/D_b$, is obtained from the tracer diffusivity, D_t, and the bulk (or charge) diffusivity D_b. Its time dependency is defined by [136],

$$H_R(t) = \sum_i <\mathbf{v}_i(0) \bullet \mathbf{v}_i(t)> / <\sum_i \mathbf{v}_i(0) \bullet \sum_j \mathbf{v}_j(t)> \tag{8.67}$$

Typical value of the Haven ratio is at around 0.2–0.5 for ionically conducting glasses and therefore the correction by this is not so large although the value gives useful information for mechanism of the transport properties. The value is known to decrease in increasing content of alkali metal, in alkali silicates or related materials [139, 140]. The ratio represents the geometric correlations in the case of single particle motion, while it is also affected by the collective or correlated motions of particles (ions) [141]. Doliwa and Heuer [142] argued that the value is an inverse of the number of particles (ions), which moves in cooperative manner. That is, typical Haven ratio means that 2–5 ions move in cooperative manner. Direct calculation of conductivity or Haven ratio from MD simulation runs were performed in some works [143, 144].

For single particle properties, statistics can be improved by taking the average of large number of particles or ions, while for collective properties such as conductivity or Haven ratio, it is not easy to obtain good statistics, especially when dealing with heterogeneous dynamics. In taking average of heterogeneous ionic motions, the use of large time windows covering different initial situations is recommended.

In principle, electric conductivity can be calculated directly from the electric current of ions, **J**(t) defined by

$$\mathbf{J} = \sum_i Q_i \dot{\mathbf{r}}_i(t), \tag{8.68}$$

where Q is the charge of the species and $\mathbf{r_i}$ is a displacement vector of the ith-ion. From the linear response theory [136], frequency dependent conductivity is given by

$$\sigma(\omega) = \frac{1}{3k_BTV} \int_0^\infty \langle \mathbf{J}(t) \bullet \mathbf{J}(0) \rangle \exp(i\omega t) dt, \tag{8.69}$$

and the direct current conductivity at the low frequency limit is given by

$$\sigma(0) = \frac{1}{3k_BTV} \int_0^\infty \langle \mathbf{J}(t) \bullet \mathbf{J}(0) \rangle dt. \tag{8.70}$$

If one compared this expression with Eq. (8.66), it is easily found that the time region for this limit corresponds to the long time limit of the MSD and/or the displacement of bulk diffusion. In the molten salt or in ionic "liquids", the time region is usually far beyond the ps region except for extremely high temperature region. At a first glance, the velocity auto-correlation function or that of the electric current might appear as if

it has converged at short time (ps) region as already mentioned. Even if apparent convergence of the auto-correlation function in a short time was found, it does not mean that the motion corresponds to low frequency limit of Eq. (8.70). Careful sampling of the data is required with considering above situations. Similar situations will be found in many systems, liquids, glasses and crystals. Some further problems for the sampling of heterogeneous and intermittent dynamics near the glass transition regimes will be discussed in Sect. 8.5.7.

8.3.2.3 Viscosity

Viscosity, η, can be obtained from the Stokes-Einstein relation [135, 145] from the diffusivity. The relation for 3D liquids is given by

$$D = k_B T / c\pi\eta R, \tag{8.71}$$

where R is the effective diameter of the particle and c is a constant. The value c is known to be 2 and 3, in slip and stick hydrodynamic boundary condition, respectively.

Near the glass transition temperature, the deviation from the Stokes-Einstein relation is often found (see Sect. 7.3.3) and fractional power law relation between D and η can be a better description (Several fractional power laws are suggested. For example, $D = A'\left(\frac{k_B T}{\eta}\right)^{\gamma}$ was assumed in Ref. [67].).

The viscosity η can be calculated from the Green-Kubo formula

$$\eta = \frac{V}{k_B T}\int_0^{\infty} dt < P_{\alpha\beta}(0) \bullet P_{\alpha\beta}(t) > \tag{8.72}$$

where αβ stands for *xy, xz, yx, yz, zx*, or *zy*, and

$$P_{\alpha\beta} = \frac{1}{V}\left[\sum_i m_i v_{i\alpha} v_{i\beta} + \sum_i \sum_{j>i} (r_{i\alpha} - r_{j\alpha}) F_{ij\beta}\right]. \tag{8.73}$$

Non Equilibrium Molecular Dynamics (NEMD) and Reverse Non-Equilibrium Molecular Dynamics (RNEMD) are also useful to derive such transport properties (see Sect. 8.6).

8.3.3 Space-Time Correlations

8.3.3.1 Self- and Distinct-Part of Van Hove Functions

Space time correlation of the particles can be brought out by the self and distinct part of van Hove functions respectively defined as follows [146, 147],

$$G_s(\mathbf{r},t) = (1/N)\sum_{i=1}^{N}\left\langle \delta\left(\mathbf{r}_i(t) - \mathbf{r}_i(0) - \mathbf{r}\right)\right\rangle \tag{8.74}$$

$$G_{\mathrm{d}}{}^{\alpha,\beta}(\mathbf{r},t) = (1/N_\alpha)\sum_{\mathrm{i}=1}^{\mathrm{N}_\alpha}\sum_{\mathrm{j}=1}^{\mathrm{N}_\beta}\left\langle \delta\left(\mathbf{r} - \mathbf{r}_i^{\alpha}(0) + \mathbf{r}_j^{\beta}(t)\right)\right\rangle \tag{8.75}$$

The former is concerned with a self-motion of a particle, while the latter is for the mutual motion of different species α and β. Usually, results in figures are shown as a function of $r = |\mathbf{r}|$. If the self-part of the van Hove function is multiplied by $4\pi r^2$, the area under the curve corresponds to the number of particle and therefore $4\pi r^2 G_{\mathrm{s}}(r)$ tends to be used for the plot.

In the distinct part of the van Hove function, new peak appears at $r = 0$ if the particle of species β comes into the site previously occupied by a particle of species α and this feature is useful to examine the jump events. (See Sects. 10.1–10.3.) During this period, structures shown by $g(r)$ are kept unchanged although at $t = 0$, the distinct part of the van Hove function is the same function as $g(r)$ of the α−β pair.

This difference of the time development is due to the fact that the origin of the coordinate is fixed on the initial position of species α in the space in the former, while relative positions of α and β species are measured in the latter.

8.3.3.2 Intermediated Scattering Functions: $F_s(k,t)$

The intermediate scattering function is defined by [147]

$$F_s(k,t) = \left\langle \sum_{j=1}^{N}\exp\left\{i\mathbf{k}\cdot\left(\mathbf{r}_j(t) - \mathbf{r}_j(0)\right)\right\}\right\rangle /N \tag{8.76}$$

The function is useful for comparison with experiments as well as many kinds of theoretical treatments in the problem of slow dynamics.

8.3.3.3 Fluctuation of the Order Parameter

Lačević et al. defined the overlap susceptibility χ_4 (which is related to the four point correlation function) as follows [148] to investigate the spatial heterogeneity in the glass forming liquids. A time dependent order parameter $Q_p(t)$, which measures the number of "overlapping particles in two configurations separated by a time interval t" is defined by

$$Q_p(t) = \int d\mathbf{r}_1 d\mathbf{r}_2 \rho(\mathbf{r}_1, 0)\rho(\mathbf{r}_2, t)\delta(\mathbf{r}_1 - \mathbf{r}_2)$$
$$= \sum_{i=1}^{N} \sum_{j=1}^{N} \delta(r_i(0) - r_j(t)), \tag{8.77}$$

where $\rho(\mathbf{r}, t) = \sum_i \delta(\mathbf{r} - \mathbf{r}_i)$.

The order parameter is related to the distinct-part of the van Hove function by, $\langle Q_p(t) \rangle = NG_d(r, t)$, with $r = 0$. In other words, this order parameter is concerned with the probability of substituting α and β species in Eq. (8.75) (for the case of single component, it is defined with $\alpha = \beta$).

The function $\chi^p{}_4(t)$, the fluctuation of the order parameter, is represented by

$$\chi^p{}_4(t) = \frac{\beta V}{N^2} [\langle Q_p^2(t) \rangle - \langle Q_p(t) \rangle^2], \tag{8.78}$$

where $\beta = (k_B T)^{-1}$.

It is rewritten as

$$\chi_4(t) = \frac{\beta V}{N^2} [\langle Q^2(t) \rangle - \langle Q(t) \rangle^2] \tag{8.79}$$

using a modified $Q(t)$ by a substitution of $\delta(\mathbf{r}_i(0) - \mathbf{r}_j(t))$ in Eq. (8.77) by the "overlap" function $w|(\mathbf{r}_1 - \mathbf{r}_2)|$. The "overlap" function is unity when $|(\mathbf{r}_1 - \mathbf{r}_2)| \leq a$ and zero otherwise. Here the parameter "a" is for typical amplitude of vibrational motion. This function can pick up the correlation length concerned with jumps or jump-like motions.

8.3.4 Thermal Properties

Thermal properties can be also determined from MD simulations. Pressure, temperature, volume, energies, and forces (each component of the kinetic and potential energies can be separated.), their time dependent behavior, and their derivatives or integral as well as fluctuations can be analyzed. In several systems such as the SC model, analytical treatment of the thermodynamic properties is possible [See Refs. [41–47] and references therein.].

8.3.5 Thermodynamic Scaling and Other Scaling Rules

The system may obey several kinds of scaling rules. Details for the thermodynamic scaling of the ionic systems are found in Chap. 7 and Sect. 11.10. Application of such rules will be helpful (see also Sect. 13.2) to predict or interpolate the properties

of materials to a different condition or state. In this manner, the scaling rules make it easier to estimate or predict the properties under a different condition, and also useful to understand the mechanism underlying them.

8.3.6 Further Possible Analyses

There are many other possible analyses of the results from MD simulations. For example, individual motion of particles (ions, molecules), rotational dynamics, 3-, 4- (or higher order) time correlation functions, details of inner and inter structures of ions or molecules, correlation among angles and/or distances, can be analyzed and examined. Furthermore, possible analyses are not limited to the ones mentioned above. One can define any kind of functions or representations. Simulations also could be done under extreme conditions such as high pressure, negative pressure, and extremely high or low temperatures. For the purpose of material designs, or examination of the mechanism of dynamics, one can change freely the mass, particle size of the constituents of the system.

8.4 Errors in the Molecular Dynamics Simulations

There are several source of errors that can occur during the MD simulations and analyses of them [149, 150]. Here we treat three kinds of errors. One is concerned with the treatment of digits in the computer. Second one is concerned with the treatment of the numerical integration during the MD runs and of the averaged quantities. The third one is concerned with the propagation of small error during MD runs related to deterministic properties of the system especially in the case of slow dynamics.

8.4.1 Errors Occurred in the Numerical Treatment

In computers, the real number with infinitive digits is approximated by the floating point numbers having a limited number of digits. There exists a round-off error due to the limit. There are several standards to treat it such as IEEE 754-2008. The value x_f can be represented by [151],

$$x_f = \pm f \times \beta^m, \quad f = \frac{x_1}{\beta} + \frac{x_2}{\beta^2} + \cdots + \frac{x_n}{\beta^n}, \tag{8.80}$$

The base for the scaling can be two, ten, or sixteen in almost all cases.

Here x_k $(k=1, \cdots, n)$ are integers with $1 \leq x_1 \leq \beta - 1$ and $0 \leq x_k \leq \beta - 1 (k = 2, \cdots, n)$.

For example, 3.14159 is represented by 0.314159×10^1. In this example, 0.314159 corresponds to the fraction f and 10 corresponds to the base, β, of the scaling and 1 corresponds to the exponent m. The parameter m is integer within the range, $L \leq m \leq U$.

The largest and the smallest values ($F_{\max}$ and $F_{\min}$), which can be treated in the machine are represented by

$$\begin{aligned} F_{\max} &= \beta^U (1 - \beta^{-n}), \\ F_{\min} &= \beta^{L-1} \end{aligned} \tag{8.81}$$

Thus the system can be characterized by β (base), n (number of significant digits), L (minimum exponent) and U (maximum exponent). These values depend on the system. For example, β = 16, n = 14, $L = -64$, and $U = 63$ may be used in the case of double precision for a certain system.

For the treatment of MD simulations, one needs to be careful for the loss of significant digits and trailing digits. The former situation occurs when the difference of comparable large values is taken. The latter situation occurs when the sum or difference of large value and extremely small value is taken.

8.4.2 Numerical Errors Occurred During MD Runs

For example, in Eq. (8.14), the third term in the right hand side of the equation is much smaller compared with other terms. To avoid the loss of trailing digits, calculation will be done by preparing the following values for $i = 1,2$ ---N

$$\Delta \mathbf{r}_i(t) = \mathbf{r}_i(t) - \mathbf{r}_i(t - \Delta t)$$

Then Eq. (8.14) was divided into two steps,

$$\Delta \mathbf{r}_i(t + \Delta t) = \Delta \mathbf{r}_i(t) + (\Delta t)^2 \frac{\mathbf{F}_i(t)}{m} \tag{8.14a}$$

and

$$\mathbf{r}_i(t + \Delta t) = \mathbf{r}_i(t) + \Delta \mathbf{r}_i(t + \Delta t) \tag{8.14b}$$

By this transformation, the values in Eq. (8.14a) become comparable in magnitude and furthermore, the error in Eq. (8.14b) will not propagate to longer times.

Pressure of the system is usually obtained from the difference of large comparable values and therefore, the loss of significant digits tends to occur. These losses as well as rounding error may be diminished by changing the order of calculations.

For example, for averaging of heterogeneous quantities for long runs, small values are better to sum up before performing the summation that includes large values. Error of the numerical integration also depends on the algorithm of the integrator used [152, 153]. For energy conservation of long time scale, symplectic integrator such as Verlet algorithm is known to be better compared with the method such as predictor-corrector method, which might be more accurate for short time runs. For the stability of the calculations, time reversible methods are also favored. Several methods with symplectic and/or time reversal properties have been proposed.

8.4.3 Propagation of Small Error and Lyapunov Exponent

As will be discussed in the Sect. 8.5 and Appendix A.2, (see also Example 2 in ESM) deterministic motion of ions causes the large fluctuation of the dynamics and such characteristics are common to other non-linear systems. Lorenz [154] has studied a predictability of non-linear dynamics of atmospheric model. In a similar manner, one can consider a propagation of the small error in MD simulations, although further problems remain as to be discussed later.

If the time evolution of the system is governed by a function $\boldsymbol{F}$ of the variables, $\boldsymbol{r}_{\mathrm{i}}(t), i = 1, \ldots, N$, in N dimensional system (i.e., the positional vectors of MD), and time evolution is determined by the following equation,

$$\frac{d}{dt}\boldsymbol{r}_i(t) = \boldsymbol{F}\left[\boldsymbol{r}_1(t), \ldots, \boldsymbol{r}_N(t)\right]; i = 1, \ldots, N, \tag{8.82}$$

The propagation of error in the basic solution, $\boldsymbol{r}_{\mathrm{i}}(t)$, beginning with initial time t_0 with a small initial error $\boldsymbol{e}_{0\mathrm{i}}$ can be approximated by the linear equations by taking the first term of the Taylor expansions,

$$\frac{d}{dt}\boldsymbol{e}_i(t) = \sum_{j=1}^{N} \frac{\partial \boldsymbol{F}}{\partial \boldsymbol{r}_j}\boldsymbol{e}_j, \tag{8.83}$$

in which the coefficient $\frac{\partial \boldsymbol{F}}{\partial \boldsymbol{r}_j}$ is time dependent.

Using Jacobian matrix of $\boldsymbol{F}$ at $\boldsymbol{r}$(t), $\left(\boldsymbol{J}_{ij} = \frac{\partial \boldsymbol{F}}{\partial \boldsymbol{r}_j}\right)$, it can be written as,

$$\frac{d}{dt}\boldsymbol{e}_i(t) = \boldsymbol{J}(\boldsymbol{r}(t))\boldsymbol{e}(t), \tag{8.84}$$

Integrating Eq. (8.84), we have at the time after τ_e of initial time,

$$\boldsymbol{e}(t_0 + \tau_e) = \boldsymbol{M}(\boldsymbol{r}(t_0), \tau_e)\boldsymbol{e}(t_0), \tag{8.85}$$

The matrix $\boldsymbol{M}$ is called as error matrix and it depends on the $\boldsymbol{r}(t)$ during this time interval.

Then one can consider the mean expansion rate of error. If initial error is randomly and spherically distributed in the N dimensional phase space, the distribution of error with size ε is represented by

$$\boldsymbol{e}^T(t_0)\boldsymbol{e}(t_0) = \varepsilon^2. \tag{8.86}$$

Here the superscript T indicates the transpose. From Eqs. (8.85) and (8.86), the distribution of error becomes an ellipsoid after τ_e, represented by,

$$\boldsymbol{e}^T(t_0+\tau_e)\left[\boldsymbol{M}(\boldsymbol{r}(t_0),\tau_e)\boldsymbol{M}^{\boldsymbol{T}}(\boldsymbol{r}(t_0),\tau_e)\right]^{-1}\boldsymbol{e}(t_0+\tau_e) = \varepsilon^2 \tag{8.87}$$

The amplification rate, α, during this time is given by [123, 155]

$$\alpha(\boldsymbol{r}(t_0),\tau_e) = \sqrt{\frac{1}{N}\sum_{i=1}^{N}\Gamma_i(\boldsymbol{r}(t_0),\tau_e)}, \tag{8.88}$$

where $\Gamma_i{=}\lambda_1{}^2,\ldots,\lambda_N{}^2$ is a N real and non-negative eigen values of the matrix $\boldsymbol{M}(\boldsymbol{r}(t_0),\tau_e)\boldsymbol{M}^{\boldsymbol{T}}(\boldsymbol{r}(t_0),\tau_e)$ and $\Gamma_{\boldsymbol{i}}{}^{1/2}$ corresponds to the local Lyapunov exponent [123, 154].

The error doubling time is inversely proportional to the leading Lyapunov exponent, a common view in the meteorological community [156]. As shown above, the error propagation in complex systems is related to the Lyapunov exponent.

There are some further problems concerning it for the above treatment. The first problem is the non-spherical distribution of the initial error, which is related to the dimensionality of the jump paths, which can be less than 3. Another problem is that the functional form of $\boldsymbol{F}$ being time dependent. Especially for slow dynamics at low temperature regions, the fluctuation of the cage in local region is larger than that for the whole system. The third problem may be a contribution of neglected terms in Eqs. (8.83) and (8.84).

8.4.4 Backward Error Analysis of the Averaged Properties

Mathematicians are interested in the numerical integration of ordinary differential equations. Backward error analysis [150, 153, 157] seems to be an important tool for understanding the long time behavior of numerical integration methods and have shown the usefulness of the symplectic integrator used in MD simulations. Traditional 'forward error analysis' describes the difference between the exact trajectory and numerical trajectory, while in the 'backward error analysis', the difference between the numerical and exact solution is expressed in terms of a perturbation of the problem or the vector field.

Bond and Leimkuhler [153] have done the backward analysis of the accuracy for numerically computed averages of MD. The history for the numerical treatment in MD was also summarized in this reference. Reich [150] has shown the long time integration of chaotic Hamiltonian systems and discussed the approximation of time averages along numerically computed trajectories. These works seem to be encouraging to use in long time MD simulations for obtaining averaged quantities.

8.5 Treatments of Slow and Fast Dynamics in Ionic Systems

Dynamics of ions in both ionically conducting glasses and ionic liquids are quite heterogeneous. That is, both fast and slow ions coexists, while the mean of the dynamics is slow, similar to dynamics of liquids in the glass transition regimes, where the rare event is not negligible. This situation makes it difficult to treat the heterogeneous dynamics in molecular dynamics simulations.

In this section, several requirements to observe such dynamics and the resultant structures will be discussed, although sometime they are difficult to fulfill by a limited calculation resource. Sampling method of such dynamics or structures is also a matter of debate here. If the system was trapped in the local metastable state on the complicated potential well, many runs with independent cooling schedule might be required. However, for the ionics with a measurable diffusivity within several ns, delayed time series with many initial times obtained by a long run, covering the phase-space, is more useful than a limited number of short time runs.

8.5.1 System Size Requirements (Relationship with Fragility and Confinement)

In MD simulations, periodic boundary condition (PBC) is often used. This is useful to treat the infinitive size of system and long ranged interactions. However, the nature of the system might be affected by the size of the basic cell. This is because the motions of particles are repeated by the periodic boundary conditions, and consequently the resultant structures also are restricted. Of course, the system size required in MD simulations depends on the problem to be treated, and researcher should select suitable size for the purpose and within the restriction of the available calculation resources. Here, some general requirements for the study of the structure and dynamics including those in the case of the silicate glasses are discussed.

8.5.1.1 General Requirements of System Size in MD

The size of the basic cell determines the largest length scale and smallest wave number accessible by MD simulations. In the case of crystal, motion of particles including vibrational mode is considerably affected by the cell size and how the unit crystal structure is repeated in the basic MD cell.

In liquids or glasses, the structure shown by pair correlation function $g(r)$, decays within a certain length. For ion-ion interactions, the correlation of the structure (deviation from the line of $g(r) = 1$) is not clear at distance longer than 8–12 Å in ionic systems such as lithium silicate glass. Therefore, twice this length is a minimum length of the unit cell for MD simulations to avoid the ionic structure being affected by the PBC. In the case of ionic liquid, longer correlation is observed as shown in Fig. 8.4. The correlation is small at around ~18 Å. Therefore the system size with ~36 Å of L will be a good choice for many purposes. However, larger system size might be necessary depends on the purpose of the simulations.

Angell has introduced a concept of "fragile" and "strong" to characterize glass forming materials [158, 159] and the system size required to examine the network glasses depends on the fragility of it. The fragile system shows a non-Arrhenius behavior, while the strong system shows an Arrhenius behavior. In the fragile liquid, the Arrhenius plot of structural relaxation time as a function of T_g/T increases rapidly near $T_g/T = 1$, and the "fragility" or fragility index m is usually defined by the slope at $T_g/T = 1$. Fragile (strong) glass-formers have large (small) value of m. In general, system size effect of the basic MD cell for dynamics is known to be larger in the "strong" system [160].

Generally, fragility is larger when the alkali content is larger and this affects the required system size of MD. For lithium silicate, experimental fragility index, m, of

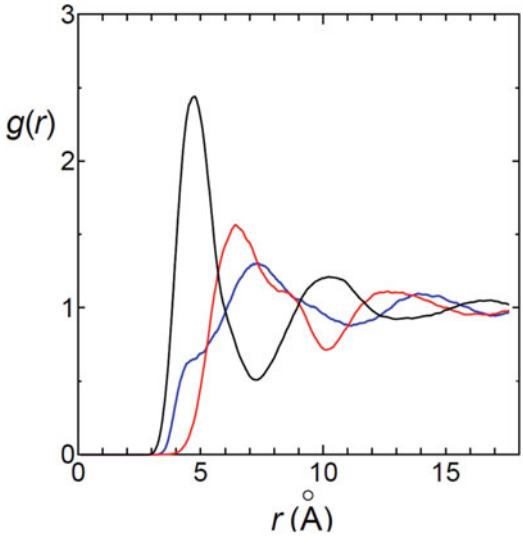

Fig. 8.4 Example of the structure of ionic liquid (EMIM-NO_3 at 400 K for system with 512 ions) examined by the center of mass positions of ions. *Black*: Cation-Anion pair, *Red*: Anion-Anion pair, *Blue*: Cation-Cation pair. Correlation of the structures is diminished but is continuing ~18 Å

silica, lithium trisilicate, lithium disilicate, and lithium metasilicate is reported to be 17.9, 26.3, 34.7 and 33.9, respectively [161]. As expected from its fragility, larger size effect on the network statistics is found in silica rich region than in the lithia rich region and therefore larger system size is required in the silica rich region.

In a confined system such as thin films, mobility of the mobile species (ions) tends to be affected by the immobile species or walls (see Sect. 10.7.1). Using the dependence of dynamics on the distance from the wall, one can obtain a length scale to characterize it. If the system is smaller compared with this length scale, particle motion is affected by its ghost particles in the image cells. Therefore this is related to the minimum size of the system required for the study of the mobile particles.

In the case of more complex systems with several domains, larger system size may be required to represent regions with different length scales. For example, in colloid-water-salt systems, domains or clusters, gels are formed by a coagulation process and the fractal dimension of local regions and connections between them are different in the cluster or gel [76].

8.5.1.2 System Size Required for the Study of Q_n Structures or Other Network Statistics

For determination of the structures in network systems with long life time, both system size dependency and cooling schedules play roles. In the case of strong system, long (and medium) ranged structure at the high temperature may remain in the system after the vitrification. As a result, the system will show the fictive glass transition temperature which depends on the cooling rate. Fixing of the high temperature structure causes a problem of how to get good statistics for the network structures. One may consider that extremely large number of runs is required to obtain statistically meaning quantity in a glass.

For the statistics of the networks, required numbers of runs may depend on the possible sub-structural units to be considered and their combinations. For Q_n (where n is the number of bridging oxygen in the SiO_4 unit) distribution in lithium disilicate, the system size (3456 particles) seems to be large enough to represent any combinations of structural units of the networks, even when the exchanges among structural units are slow. If one would like to examine the structures at longer range such as the connectivity of the Q_n units, larger size may be required. Some differences of the distribution are found by each quenching schedule and ensemble due to the existence of polyamorphism (see Sect. 9.2 for more details). In a limiting case of high pressure region, the statistics of the distribution can be well represented by the binomial distribution as a first approximation [134, 162] and this resulted in good reproducibility of the structures and dynamics of ions in the glassy state from the works of different researchers.

Thus the system sizes should be large enough for the purpose of simulations. However, due to practical reasons such as the calculation time, the required storage and the cost, extremely large system is not necessarily recommended. One should consider the balance of several factors to choose the condition of simulations.

8.5.2 Equilibration and Cooling Schedules in the MD Simulation of Glasses

Generally, different length scale motions have different time scales and therefore larger system requires longer equilibration time. Some characteristics observed near the glass transition of the system can be understood by existence of these different time scales of substructures.

When the temperature or pressure of the system is changed, shorter length scale motion of local structure can rapidly follow it, while the longer length scale motion of long ranged structure occurs after that. For example, formation of glass starts from short length scale, and spreads to the long length scale [163]. As a result, the system near T_g shows some cooling rate dependence. Actually, Vollmayr et al. [164] found that the glass transition temperature T_g in silica is in accordance with a logarithmic dependence on the cooling rate γ. The rate γ seems to have a much more marked effect on the radial distribution function, the bond-bond angle distribution function, the coordination numbers, and the distribution function for the size of the rings, than density and thermal expansion coefficients. Recently, Forero-Martinez et al. [165] found the trend such as $T_g(vol) > T_g(ene)$ (vol and ene stand for volume and energy, respectively.) for the glass transition temperatures in ionic liquids and it was rationalized in terms of the different relaxation times of energy and volume. It was pointed out that the volume is an intrinsically N-body property, depending on the relative position of far-away particles, while energy depends primarily on the local arrangement of particles, whose relaxation in response to temperature variations is faster than in the case of volume. As a result, energy provides an estimate of T_g somewhat less affected than $T_g(vol)$ by fast quenching rates. Thus the cooling schedule should be designed with considering the different length scales. It is probable that reproducibility of the glass transition temperature becomes better, if the system was maintained just above the glass transition regimes for a long time and then the system was cooled down further. In this condition, long (and medium) ranged structures are equilibrated enough and glass transition temperature is determined mainly by the short length scale structures.

8.5.3 Ensembles Used in the Simulations of Super-Cooled Liquid, Glass, and in the Treatment of Glass Transition

Mostly experiments have been done under constant pressure conditions; while constant energy condition (micro canonical ensemble) is obtained in MD, as long as one does not use modification by additional degrees of freedom. Therefore, the extended ensembles are useful for direct comparison of MD and experiments for some purposes. However, details of the thermodynamics (and its fluctuation) and motion of particles near the glass transition regimes depends on the ensemble used. Therefore suitable conditions should be chosen dependent on the purpose.

When the system is sensitive for thermodynamic condition in the preparation of glass, question arises is what condition should be used in the study of glass transition. So far, many MD works for the glass transition seem to be done in the fixed volume condition and structures prepared in such a manner are not the same as that obtained at ambient pressure. There are reasons to select such conditions. Binder [166] pointed out that "It is essential to carry out simulations for examining the glass transition at constant density (taken from experiment) and not at constant pressure, because in the latter case, there is a too strong dependence of the simulated properties on the cooling rate of the simulation." It seems to be reasonable for those with this point of views. Still one may ask how the system depends on the volume change during the cooling schedule, because the strong dependence can be characteristics of the glass transition.

As will be shown for the Q_n distribution of the network of the silicates (see Sect. 9.2), it depends on the pressure or volume of the system considerably. This is explained by the fact that a local structural unit has its own specific volume as already mentioned. Furthermore, the system may show polyamorphism [167] in the certain region of the phase-diagram [134]. Therefore, the resultant structure of glasses depends on the path on the P-V-T diagram during the cooling schedules.

Since the different ensemble causes differences in the pathway and direction of the fluctuation on the phase-diagram during the non-equilibrium relaxation as shown for SC model [45, 46, 168], caution should be paid to the ensembles used during the cooling schedules.

Thus, one of the possible choices comparable to experiments may be the following conditions. The cooling is performed by constant pressure conditions with temperature scaling or gradual changes in temperatures and the following run is performed in the NVE condition at each target temperature and under a target pressure. If the temperature spontaneously increases during NVE runs, it means the system is under the non-equilibrium relaxation (aging) [45]. Therefore, further control of temperature may be necessary during this period. An NPT ensemble will be also useful, if the overlap with the aging is small or distinguished clearly.

8.5.4 Sampling of Structures and Dynamics Near the Glass Transition Regimes and Glasses

For adequate sampling of the structure of glasses and jump motions including cooperative ones, long time scale simulations and large system size are required especially near the glass transition regimes. Here adequate sampling means that the trajectories cover whole region in the phase space. In other words, the effective sampling is concerned with the "ergodicity" of the system. For MD performed for a limited time scale, is this condition achieved? Is the system trapped in a certain position in the phase space? Fortunately as shown in Sect. 9.9, the transport

properties of ions obtained MD are comparable to the experimental ones and such sampling seems to be possible. This is understandable as discussed in the following subsections.

8.5.5 Non-ergodicity of the Dynamics for Network Former

At first, we consider the case of network former in the silicate glass as an example. Since the reconstruction of Si-O bonding is a slower process than ionic motion, it will be more affected by the cooling rate and the characteristics of the structure in the molten state will remain in the structures of glasses. That is, their structures are affected by the fictive temperature as known in experiments. Due to this reason, network structure represented by Q_n (n means number of bridging oxygen atoms in a SiO_4 unit) distribution shows large fluctuations in each quenching run. However, the rearrangement of Si-O bonding is relatively fast process above the glass transition temperature (for example at 1000 K in lithium disilicate, rearrangement occurs within several tens ps), in the conventional MD system with a periodic boundary condition. Thereby one can obtain quasi-equilibrated Q_n distribution, which is approximately represented by the binomial distributions. This means that the different substructures of the network is mixed well and can be sampled enough in these systems. (See Sect. 9.2 for more details for the observed Q_n distribution). If one examined the structure of longer length scale (such as rings), larger system size and longer relaxation time may be required. However, at least for examining the ionics in the system, non-ergodicity of the network structure does not cause severe problems. If suitable cooling schedules are used, reproducibility of dynamics is also good. (See Sect. 9.9 for the comparison of ion dynamics in MD and experiments.) This fact implies that the effect of rapid cooling rate in MD is compensated by the system size effect with periodic boundary conditions at least partially.

8.5.6 Relation Between Ion Dynamics and Chaos

Even for ionic motion, obtaining good statistics in slow dynamics is sometimes a difficult task due to strong heterogeneity with intermittency of the jump motions. At first, here we discuss how ion dynamics are related to the deterministic chaos to understand such characteristics of ionic motions. In the super-cooled liquid states or in the glass, the motion of ions occurs through jump motions among ionic sites (see Sect. 2.4 for examples of such motions in ionic systems). Larger fluctuation of the ion dynamic is observed compared with simple liquids. Similar situation occurs in the ionic liquids, molten salt, crystals, bio-materials, colloidal systems and so on.

Strong heterogeneity with intermittency mentioned above is related to the deterministic character of the motion.

Researchers may encounter such motion even in a simple system such as the SC model [46] or the Lennard-Jones model [168, 169]. Simonazzi and Tenenbaum [169] have reported that the kinetic energy fluctuations exhibit an anomalous behavior in LJ microcrystals at low temperature and attributed them due to weak chaos. Deterministic nature of the system resulted in the intermittent and sporadic behaviors [171] frequently observed near the glass transition regimes.

8.5.7 Sampling of Rare Event with Dynamic Heterogeneity-Ergodicity of Ionic Motion

For ionics in the glassy state, system shows exchanges between vast or laminar states and cooperative motions of several ions emphasize such a behavior [172]. For averaging such properties, many independent initial positions and/or wide time window are required [173], if the calculation resources and times allow it to be performed. Deterministic behaviors of the system are also found in extended ensembles. Holian et al. [174] have pointed out that the Toda "demon" is hidden in the Nosé-Hoover thermostat, which can cause the noncanonical undulations. Therefore, if one used extended dynamics, it is better to check if the dynamics are affected by it or not. In the case of slow dynamics, sampling of the rare events such as cooperative motions of several ions is always problematic [17, 171]. It also means the difficulty of averaging the heterogeneous dynamics.

How can we cover the wide region of the phase-space and how can we check it? One possible method to cover the wide phase-space is using a lagged time series as shown below. To reduce the effect of fluctuation of dynamic heterogeneity related to the cooperative nature of jumps for statistic treatment of the system, average for many number of lagged time series, $\mathbf{r}(t)$, $\mathbf{r}(t+\tau'')$,$\cdots\cdots$ and $\mathbf{r}(t+(m-1)\tau'')$, can be used for the analysis of MD data. Large time windows and many initial times are required because MD trajectories have correlations between successive motions. If the time window, $m\tau''$, covered by the many initial times is wide enough, long correlated motion with strong dynamic heterogeneity can be smoothed out. This procedure using lagged time series is similar to the "embedding" [175, 176] to find out the deterministic chaos in the time series. That is, the procedure can cover the trajectories in the phase-space.

Once sampling time is long enough with wide time windows, results of transport properties of ions obtained by different runs starting from different configurations or those by different researchers are comparable when the same potential model and comparable cooling schedule was used. This suggests that the long time ionic motion in ionically conducting glasses has "ergodicity" at least approximately, once the whole phase-space structure can be covered during the observation time. By this method, one can reproduce well the transport properties such as diffusion coefficient of ions.

Exceptional case is observed at quite low temperatures, where the aging (non-equilibrium relaxation) overlaps the observed dynamics. If permanently trapped particle exists, non-ergodicity of the dynamics might be found.

Of course, accumulation of independent runs is one of the possible choices for the sampling method. However, how may runs are required for this kind of sampling?

In Fig. 8.5, the van Hove functions of cations in the ionic liquid, EMIM-NO_3 obtained at 370 K, which shows a medium degree of heterogeneity is compared with the randomly sampled data from the original curve in (a). The shape strongly depends on the number of the samples, N_S. Many independent samples are required

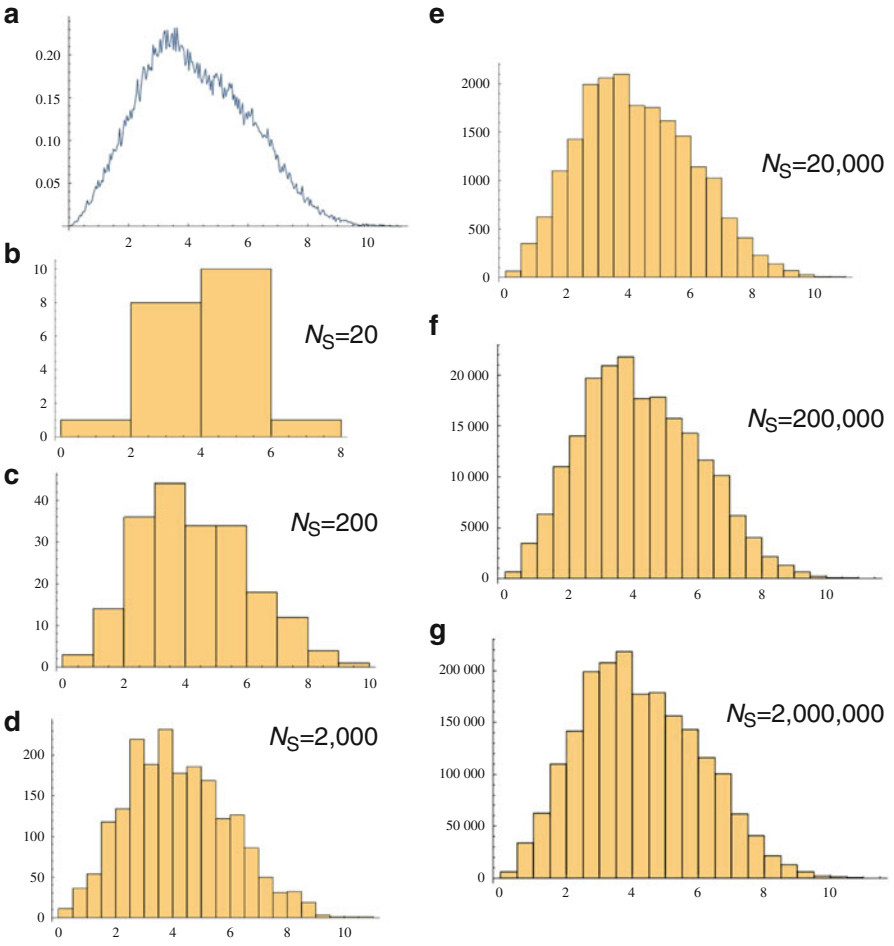

Fig. 8.5 (**a**) Distribution curve taken from the self-part of the van Hove functions of cations in EMIM-NO_3 at 370 K at 2.5 ns determined by using many lagged time series. (**b**)–(**g**) Reproducibility of the functional form by random sampling from the original distribution, where N_s data points are used. Many data points are necessary to reproduce the original functional form

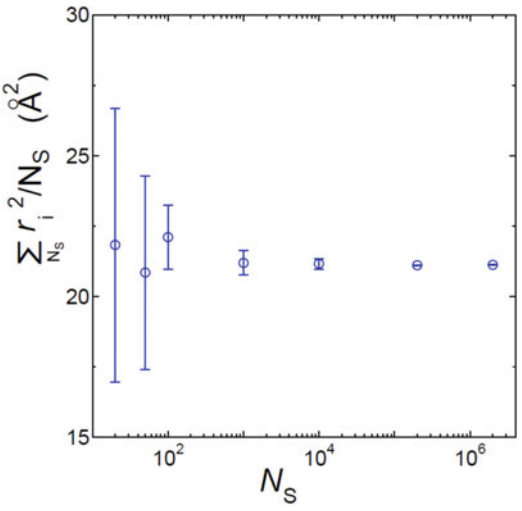

Fig. 8.6 Dependence of mean squared displacement on number of random sampling, N_S. Error bars are obtained from three or four runs using different random numbers. Distribution is taken from the same original function shown in Fig. 8.5a

to reproduce the original curves including power law tail and an exponential truncation.

In Fig. 8.6, the mean squared displacement at 2.5 ns calculated from reproduced distributions was plotted against N_S. Error bars are for three or four examples with the same N_s. For obtaining the mean value, ~10^4 of N_S may be enough; while to reproduce the functional form in details, more than 10^5 independent samples are required. More heterogeneous the system, the larger number of samples will be required. It is not easy to do so many runs and furthermore, independent short time runs are not necessarily better than the small number of long runs to understand the dynamics of the system. This is because they cannot cover the low frequency mode, which is responsible for the transport properties of the glass and they cannot recover the functional form concerned with the slow dynamics. Long time run is also useful for sampling of rare events. If the observation time is not long enough, it is difficult to observe the rare events such as correlated motion of ions of long time scales in spite of the fact that its contribution to the dynamic properties are non-negligible.

For the single particle motions, sampling for the space can be done by many ions spread out in the system. Therefore the average can be taken for many ions. Existence of the large fluctuation is more serious problem for the collective motion compared with the single particle motion. For example, enhanced heterogeneity seems to be observed for molecular motion in bio-systems, where a small number of molecules or units tend to be treated.

The cooling rate dependency of ion dynamics is smaller compared with that of network [177] due to higher relaxation rate, but still it is non-negligible when it is accompanied with the relaxation of networks. (See Sect. 9.9.)

8.6 Non-equilibrium Molecular Dynamics and Reverse Non-equilibrium Molecular Dynamics

In slow dynamics, it is not easy to attain the region of constant transport coefficient in MSD or other dynamic properties. In such a case, Non-Equilibrium Molecular Dynamics, NEMD can be useful. In this method, the system is treated by the external force such as that giving rise to shear viscosity [178]. Reverse Non-Equilibrium Molecular Dynamics [179, 180], RNEMD, is also useful for investigating the transport properties of glass-forming systems, because it provides faster convergence than the usual numerical non-equilibrium or equilibrium methods. The RNEMD method is based on the phenomenological relation:

$$J_Z(p_x) = -\eta\left(\frac{\partial v_x}{\partial z}\right), \tag{8.89}$$

where $\left(\frac{\partial v_x}{\partial z}\right)$ is the shear, $J_Z(p_x)$ is the transverse momentum flux, and η is the shear viscosity. In this method, different from the usual techniques, $J_Z(p_x)$ is **imposed** and the shear is **measured**.

References

1. L.V. Woodcock, Phys. Chem. Lett. **10**, 257 (1971)
2. F.G. Fumi, M.P. Tosi, J. Phys. Chem. Solids **25**, 31 (1964)
3. M.P. Tosi, F.G. Fumi, J. Phys. Chem. Solids **25**, 45 (1964)
4. A. Rahman, R.H. Fowler, A.H. Narten, J. Chem. Phys. **57**, 1 (1972)
5. L.V. Woodcock, C.A. Angell, P. Cheeseman, J. Chem. Phys. **65**, 1565 (1976)
6. T.F. Soules, J. Non-Cryst. Solids **49**, 29 (1982)
7. L.V. Woodcock, K. Singer, Trans. Faraday Soc. **67**, 12 (1971)
8. S. Tsuneyuki, M. Tukada, M. Aoki, Y. Matsui, Phys. Rev. Lett. **61**, 869 (1988)
9. S. Tsuneyuki, Thesis of Ph. D of physics, University of Tokyo, 1989
10. C.R.A. Catlaw, G.D. Price, Nature **347**, 243 (1990)
11. H. Ogawa, Y. Shiraishi, K. Kawamura, T. Yokokawa, J. Non-Cryst, Non-Cryst. Solids **119**, 151 (1990)
12. J. Habasaki, I. Okada, Mol. Simul. **9**, 319 (1992)
13. J. Habasaki, I. Okada, Y. Hiwatari, J. Non-Cryst. Solids **183**, 12 (1995)
14. J. Habasaki, I. Okada, Y. Hiwatari, J. Non-Cryst. Solids **208**, 181 (1996)
15. J. Habasaki, K.L. Ngai, Y. Hiwatari, J. Chem. Phys. **121**, 925 (2004)
16. J. Habasaki, K.L. Ngai, Y. Hiwatari, C.T. Moynihan, J. Non-Cryst. Solids **349**, 223 (2004)
17. J. Habasaki, I. Okada, Y. Hiwatari, Phys. Rev. **B55**, 6309 (1997)
18. J. Habasaki, I. Okada, Y. Hiwatari, Phys. Rev. **E52**, 2681 (1995)
19. H. Lammert, M. Kunow, A. Heuer, Phys. Rev. Lett. **90**, 215901 (2003)
20. C. Mueller, E. Zienicke, S. Adams, J. Habasaki, P. Maass, Phys. Rev. **B75**, 014203 (2007)
21. R.A. Montani, C. Balbuena, M.A. Frechero, Solid State Ion. **209–210**, 5 (2012)
22. L.G.V. Gonçalves, J.P. Rino, J. Non-Cryst. Solids **402**, 91 (2014)
23. G.N. Greaves, Solid State Ion. **105**, 243 (1998)

24. P. Jund, W. Kob, R. Jullien, Phys. Rev. B **64**, 134303 (2001)
25. J. Horbach, W. Kob, Phys. Rev. B **60**, 3169 (1999)
26. A.N. Cormack, Top. Mol. Organ. Eng. **15**, 227 (2002)
27. A.N. Cormack, J. Du, T.R. Zeitler, Phys. Chem. Chem. Phys. **4**(14), 3193 (2002)
28. J. Du, R. Devanathan, L.R. Corrales, W.J. Weber, Comput. Theor. Chem. **987**, 62 (2012)
29. A. Tilocca, Phys. Rev. B **76**, 224202 (2007)
30. R.S. Payal, S. Balasubramanian, Phys. Chem. Chem. Phys. **16**, 17458 (2014)
31. J. Habasaki, K.L. Ngai, J. Chem. Phys. **129**, 194501 (2008)
32. C.Y. Ouyang, S.Q. Shi, Z.X. Wang, H. Li, X. J. Huang, L.Q. Chen, Europhys. Lett. **67**, 28 (2004)
33. S. Ispas, T. Charpentier, F. Mauri, D.R. Neuville, Solid State Sci. **12**, 183 (2010)
34. A. Tilocca, J. Chem. Phys. **133**, 014701 (2010)
35. A. Tilocca, N.H. de Leeuw, J. Mater. Chem. **16**, 1950 (2006)
36. M.G. Del Pópolo, R.M. Lynden-Bell, J. Kohanoff, J. Phys. Chem. B **109**, 5895 (2005)
37. A. Carré, J. Horbach, S. Ispas, W. Kob, EPL **82**, 17001 (2008)
38. R. Car, M. Parrinello, Phys. Rev. Lett. **55**, 2471 (1985)
39. Y. Wang, W.G. Noid, P. Liu, G.A. Voth, Phys. Chem. Chem. Phys. **11**, 2002 (2009)
40. D. Jeong, M.Y. Choi, H.J. Kim, Y. Jung, Phys. Chem. Chem. Phys. **12**, 2001 (2010)
41. W.G. Hoover, M. Ross, K.W. Johnson, D. Henderson, J.A. Barker, B.C. Brown, J. Chem. Phys. **52**, 4931 (1970)
42. Y. Hiwatari, H. Matsuda, T. Ogawa, N. Ogita, A. Ueda, Progress Theor. Phys. **52**, 1105 (1974)
43. M. Tanemura. Y. Hiwatari, H. Matsuda, T. Ogawa, N. Ogita, A. Ueda, Progress Theor. Phys. **58**, 1079 (1977); ibid. **58**, 3070 (1977)
44. A. Ueda, Butsuri **62**, 769 (2007). in Japanese
45. J. Habasaki, A. Ueda, J. Chem. Phys. **134**, 084505 (2011)
46. J. Habasaki, A. Ueda, J. Chem. Phys. **138**, 144503 (2013)
47. M. Tanemura, H. Matsuda, T. Ogawa, N. Ogita, A. Ueda, J. Non-Cryst. Solid **117/118**, 883 (1990)
48. J. Habasaki, R. Casalini, K.L. Ngai, J. Phys. Chem. B **114**, 3902 (2010)
49. F. Simon, F. Lange, Z. Physik, **38**, 227 (1926)
50. G.E. Gibson, G.S. Parks, W.M. Latimer, J. Am. Chem. Soc. **42**, 1542 (1920)
51. G.S. Parks, J. Am. Chem. Soc. **47**, 338 (1925)
52. B. Bernu, Y. Hiwatari, J.P. Hansen, J. Phys. C **18**, L371 (1985)
53. T. Muranaka, Y. Hiwatari, J. Phys. Soc. Jpn. **67**, 1982 (1998)
54. J. Matsui, T. Odagaki, Y. Hiwatari, Phys. Rev. Lett. **73**, 2452 (1994)
55. T. Mizuguchi, T. Odagaki, Phys. Rev. E **79**, 051501 (2009)
56. E.A. Jagla, Phys. Rev. **E63**, 061509 (2001)
57. J.E. Lennard-Jones, Proc. R. Soc. Lond. A **106**, 463 (1924)
58. D. Brown, J.H.R. Clarke, Mol. Phys. **51**, 1243 (1984)
59. J.A. White, J. Chem. Phys. **111**, 9352 (1999)
60. G. Mie, Ann. Physik. Lpz. **11**, 657 (1903)
61. M. Edalat, S.S. Lan, F. Pang, G.A. Mansoori, Int. J. Thermophys. **1**, 177 (1980)
62. W. Kob, H.C. Andersen, Phys. Rev. **E51**, 4626 (1995)
63. P. Bordat, F. Affouard, M. Descamps, K.L. Ngai, Phys. Rev. Lett. **93**, 105502 (2004)
64. P. Bordat, F. Affouard, M. Descamps, K.L. Ngai, J. Non-Cryst. Solids **352**, 4630 (2006)
65. J. Habasaki, K.L. Ngai, Phys. Chem. Chem. Phys. **9**, 4673 (2007). and references cited therein
66. L.C. Valdes, F. Affouard, M. Descamps, J. Habasaki, J. Chem. Phys. **130**, 154505 (2009)
67. J. Habasaki, F. Affouard, M. Descamps, K.L. Ngai, IAP Proc. **982**, 154 (2008)
68. F.G. Fumi, M.P. Tosi, J. Phys. Chem. Solids **25**, 31 (1964)
69. T.L. Gilbert, J. Chem. Phys. **49**, 2640 (1968)
70. Ida, Phys. Earth Planet Inter. **13**, 97 (1976)
71. M.G. Del Pópolo, G.A. Voth, J. Phys. Chem. **B108**, 1744 (2004)

72. T.I. Marrow, E.J. Maginn, J. Phys. Chem. **B106**, 12807 (2002)
73. J.N.C. Lopes, J. Deschamps, A.A.H. Pa'dua, B**108**, 2038 (2004)
74. A.C.T. van Duin, A. Strachan, S. Stewman, Q. Zhang, X. Xu, W.A. Goddard III, J. Phys. Chem. **107**, 3803 (2003)
75. H. Manzano, S. Moeini, F. Marinelli, A.C.T. van Duin, F.-J. Ulm, R.J.-M. Pellenq, J. Am. Chem. Soc. **134**, 2208 (2012)
76. J. Habasaki, M. Ishikawa, Phys. Chem. Chem. Phys. **16**, 24000 (2014)
77. H.J.C. Berendsen, J.P.M. Postma, W.F. van Gunsteren, J. Hermans, in *Intermolecular Forces*, ed. by B. Pullman (Reidel, Dordrecht, 1981), p. 331
78. H.J.C. Berendsen, J.R. Grigera, T.P. Straatsma, J. Phys. Chem. **91**, 6269 (1987)
79. M.W. Mahoney, W.L. Jorgensen, J. Chem. Phys. **112**, 8910 (2000)
80. S.W.A. Rick, and references therein. J. Chem. Phys. **120**, 6085 (2004)
81. J. Zielkiewicz, J. Chem. Phys. **123**, 104501 (2005)
82. M.W. Mahoney, W.L. Jorgensen, J. Chem. Phys. **114**, 363 (2001)
83. V.A. Bakaev, W.A. Steele, J. Chem. Phys. **111**, 9803 (1999)
84. L. Verlet, Phys. Rev. **159**, 98 (1967)
85. In the symplectic integrator, time propagator is decomposed into a product of easily obtainable propagators, where each time evolution can be solved rigorously. The methods are known to conserve energy for long time; J.M. Sanz-Serna, *Proceedings of the International Congress of Mathematicians, Zürich, Switzerland 1994* © (Birkhäuser Verlag, Basel, 1995)
86. S. Nosé, J. Phys. Soc. Jpn. **70**, 75 (2001)
87. M.P. Allen, D.J. Tildesley, *Computer Simulation of Liquids* (Oxford University Press, New York, 1989)
88. E. Madelung, Phys. Z. **19**, 524 (1918)
89. K.S. Thorne, Rev. Mod. Phys. **52**, 299 (1980)
90. P.P. Ewald, Ann. Phys. **64**, 253 (1921)
91. A. Ueda, *Molecular Simulations -from Classical to Quantum Method* (SHOKABO, Tokyo, 2003). in Japanese
92. C. Kittel, *Introduction to Solid State Physics*, 5th edn. (Wiley, New York, 1976)
93. R.J.W. Eastwood, L. Hockey, D.N. Lawrence, Comput. Phys. Commun. **19**, 215 (1980)
94. W. Eastwood, L. Hockey, *Computer Simulation Using Particles* (McGraw-Hill, New York, 1985)
95. T. Darden, D. York, L. Pedersen, J. Chem. Phys. **98**, 10089 (1993)
96. For example, see Toukmaji, J.A. Board Jr. Comput. Phys. Commun. **95**, 73 (1996); http://www.ccp5.ac.uk/DL_POLY_CLASSIC/FAQ/FAQ2.shtml The address is confirmed to be valid on 14th Feb. 2016
97. J.E.L. Barnes, P. Hut, Nature **324**, 446 (1986)
98. V. Greengard, J. Rokhlin, Comput. Phys. **73**, 325 (1987)
99. T.J. Giese, D.M. York, J. Comput. Chem. **29**, 1895 (2008)
100. J. Carrier, L. Greengard, V. Rokhlin, SIAM J. Sci. Stat. Comput. **9**, 669 (1988)
101. E.T. Newman, R. Penrose, Phys. Rev. Lett. **15**, 231 (1965)
102. P.J. Steinhardt, D.R. Nelson, M. Ronhetti, Phys. Rev. B **28**, 784 (1983)
103. W. Dieterich, P. Maass, Solid State Ion. **180**, 446 (2009)
104. J. Habasaki, Mol. Phys. **70**, 513 (1990)
105. K.L. Ngai, J. Habasaki, J. Chem. Phys. **141**, 114502 (2014)
106. J. Habasaki, K.L. Ngai, J. Chem. Phys. **142**, 164501 (2015)
107. *The Molecular Dynamics of Liquid Crystals*, ed. by G.R. Luckhurst, C.A. Veracini (Kluwer, Nato Science Series C 1994)
108. H. Goldstein, *"The Euler Angles" and "Euler Angles in Alternate Conventions." in Classical Mechanics*, 2nd edn. (Addison-Wesley, 1980), pp. 143 and 606
109. W.R. Sir, *Hamilton, Lectures on Quaternions* (Hodges & Smith, Dublin, 1853)
110. H.C. Andersen, J. Chem. Phys. **72**, 2384 (1980)
111. S. Nosé, Mol. Phys. **52**, 511 (1984)

112. W.G. Hoover, Phys. Rev. **A31**, 1695 (1985)
113. J.M. Haile, S. Gupta, J. Chem. Phys. **79**, 3067 (1983)
114. S.D. Bond, B.J. Leimkuhler, B.B. Laird, J. Comput. Phys. **151**, 114 (1999)
115. J.M. Thijssen, *Computational Physics* (Cambridge University Press, 1999)
116. M. Parrinello, A. Rahman, Phys. Rev. Lett. **45**, 1196 (1980)
117. A. Rahman, N. Parrinello, J. Appl. Phys. **52**, 7182 (1981)
118. J.R. Ray, A. Rahman, J. Chem. Phys. **80**, 4423 (1984)
119. A.L. Loeb, *Space Structures* (Addison-Wesley, 1976)
120. J. Makino, M. Taiji, *Simulations with Special-Purpose Computers* (Wiley, 1997)
121. J. Habasaki, K.L. Ngai, to be published
122. E.N. Lorenz, J. Atoms. Sci. **20**, 130 (1963)
123. S. Yoden, M. Nomura, J. Atmos. Sci. **50**, 1531 (1993)
124. P. Keblinski, J. Eggebrecht, D. Wolf, S.R. Phillpot, J. Chem. Phys. **113**, 282 (2000)
125. B.P. Lee, M.E. Fisher, Europhys. Lett. **39**, 611 (1997)
126. M.G. Del Pópolo, G.A. Voth, J. Phys. Chem. B **108**, 1744 (2004)
127. J. Habasaki, K.L. Ngai, J. Non-Cryst. Solids **357**, 446 (2011)
128. D. Chandler, *Introduction to Modern Statistical Mechanics* (Oxford University Press, New York, 1987)
129. J.P. Hansen, I.R. MacDonald, *Theory of Simple Liquids*, 2nd edn. (Academic, London, 1990)
130. C.G. Gray, K.E. Gubbins, *Theory of Molecular Fluids*, vol 1 (Clarendon, Oxford, 1984)
131. S.K. Chatterjee, *X-ray Diffraction: Its Theory and Applications* (PHI Learning, 2010)
132. Y. Waseda, E. Matsubara, K. Shinoda, *X-Ray Diffraction Crystallography: Introduction, Examples and Solved Problems* (Springer, 2011)
133. H. Doweidar, J. Non Cryst. Solids **194**, 155 (1996)
134. J. Habasaki, K.L. Ngai, J. Chem. Phys. **139**, 064503 (2013)
135. A. Einstein, *Investigations on the Theory of Brownian Motion* (Dover, New York, 1956)
136. R. Kubo, J. Phys. Soc. Jpn. **12**, 570 (1957)
137. T. Odagaki, M. Lax, Phys. Rev. B **24**, 5284 (1981)
138. Y. Haven, B. Verkerk, Phys. Chem. Glasses **6**, 38 (1965)
139. G.E. Murch, Solid State Ionics **7**, 177 (1982)
140. J.O. Isard, J. Non-Cryst. Solids **246**, 16 (1999)
141. B. Hafskjold, X. Li, J. Phys. Condens. Matter **7**, 2949 (1995)
142. B. Doliwa, A. Heuer, Phys. Rev. E **61**, 6898 (2000)
143. G.A. Evangelakis, V. Pontikis, Europhys. Lett. **8**, 599 (1989)
144. A. Heuer, M. Kunow, M. Vogel, R.D. Banhatti, Phys. Chem. Chem. Phys. **4**, 3185 (2002)
145. Some researchers suggest to call it Stokes-Einstein-Sutherland relation. See, W. Sutherland, Phil. Mag. **9**, 781 (1905)
146. A. Rahman, K.S. Singwi, A. Sjolander, Phys. Rev. **126**, 986 (1962)
147. L. Van Hove, Phys. Rev. **95**, 249 (1954). The same basic ideas were earlier put forward by Glauber. R.J. Glauber, Phys. Rev. **8**7, 189 (1952); **94**, 751 (1954); **98**, 1692 (1955)
148. N. Lačević, T.B. Schrøder, F.W. Starr, S.C. Glotzer, J. Chem. Phys. **119**, 7372 (2003)
149. R.A. Lippert, K.J. Bowers, R.O. Dror, M.P. Eastwood, B.A. Gregersen, J.L. Klepeis, I. Kolossvary, J. Chem. Phys. **126**, 046101 (2007)
150. S. Reich, SIAM J. Numer. Anal. **36**, 1549 (1999)
151. M. Sugihara, K. Murota, "Mathematical principle of numerical calculation methods", second version (in Japanese. The title was translated.), Iwanami, 1994. ISBN4-00-005518-6
152. S. Toxvaerd, O.J. Heilmann, T. Ingebrigtsen, T.B. Schrøder, J.C. Dyre, J. Chem. Phys. **1**, 064102 (2009)
153. S.D. Bond, B.J. Leimkuhler, Acta Numer. **16**, 1 (2007)
154. E.N. Lorenz, J. Atoms. Sci. **20**, 130 (1963)
155. H. Mukougawa, M. Kimoto, S. Yoden., J. Atmos. Sci. **48**, 1231 (1991)
156. E.N. Lorenz, *Predictability –a Problem Partly Solved. Predictability,* ed. by T. Palmer, European Center for Medium Range Forecasting, (Shinfield Park, Reading, 1996);

Predictability of Weather and Climate, ed. by T. Palmer, R. Hagedorn, (Cambridge University Press, 2006)
157. G. Benettin, A. Giorgilli, On the Hamiltonian interpolation of near to the identity Symplectic mappings with application to symplectic integration algorithms. J. Statist. Phys. **74**, 1117 (1994)
158. C.A. Angell, J. Non-Cryst. Solids **73**, 1 (1985)
159. R. Böhmer, K.L. Ngai, C.A. Angell, D.J. Plazek, J. Chem. Phys. **99**, 4201 (1993)
160. J. Horbach, W. Kob, K. Binder, C.A. Angell, Phys. Rev. E. **54**, R5897 (1996)
161. M.L.F. Nascimento, C. Aparicio, J. Phys. Chem. Solids **68**, 104 (2007)
162. E.D. Lacy, Phys. Chem. Glasses **6**, 171 (1965)
163. J. Habasaki, Mol. Phys. **1990**, 513
164. K. Vollmayr, W. Kob, K. Binder, Phys. Rev. B **54**, 15808 (1996)
165. N.C. Forero-Martinez, R. Cortes-Huerto, P. Ballone, J. Chem. Phys. **136**, 204510 (2012)
166. K. Binder, J. Non-Cryst. Solids **274**, 332 (2000)
167. O. Mishima, L.D. Calvert, E. Whalley, Nature **314**, 76 (1985)
168. J. Habasaki, A. Ueda, J. Non-Cryst. Solids, **447**, 212 (2016)
169. R. Simonazzi, A. Tenenbaum, Phys. Rev. E54, 964 (1996)
170. F. Calvo, J. Chem. Phys. **108**, 6861 (1998)
171. X.-J. Wang, Phys. Rev. A**45**, 8407 (1992)
172. J. Habasaki, Y. Hiwatari, Phys. Rev. **E59**, 6962 (1999)
173. J. Habasaki, Y. Hiwatari, Phys. Rev. **E65**, 021604 (2002)
174. B.L. Holian, A.F. Voter, R. Ravelo, Phys. Rev. **E52**, 2338 (1995)
175. The method of "embedding" is used to reconstruct the attractor of the non-linear motion; N.H. Packard, J.P. Crutchfield, J.D. Farmar, R.S. Shaw, Phys. Rev. Lett. **45,** 712 (1980)
176. F. Takens, Dynamical Systems and Turbulence, Warwick 1980 (Coventry, 1979/1980), Lecture Notes in Mathematical, vol 898 (Springer, Berlin, 1981), pp. 366–381
177. J. Tilocca, Chem. Phys. **139**, 114501 (2013)
178. G. Ciccotti, G. Jacucci, Phys. Rev. Lett. **35**, 789 (1975)
179. P. Bordat, F. Müller-Plathe, J. Chem. Phys. **116**, 3362 (2002)
180. P. Bordat, F. Affouard, M. Descamps, F. Müller-Plathe, J. Phys. Condens. Matter **15**, 5397 (2003)